Kinetics, selectivity and scale up of the Fischer-Tropsch synthesis

van der Laan, Gerard Pieter

2

Kinetics and Selectivity of the Fischer-Tropsch Synthesis. A Literature Review

Abstract

A critical review is given on the kinetics and selectivity of the Fischer-Tropsch synthesis. The focus is on reaction mechanisms and kinetics of the water gas shift and Fischer-Tropsch reactions. New developments in the product selectivity as well as the overall kinetics are reviewed. It is concluded that the development of rate equations for the FTS should be based on realistic mechanistic schemes. Qualitatively, there is agreement that the product distribution is affected by the occurrence of secondary reactions (hydrogenation, isomerization, reinsertion, and hydrogenolysis). At high CO and H_2O pressures, the most important secondary reaction is readsorption of olefins resulting in initiation of chain growth processes. Secondary hydrogenation of olefins may occur at high hydrogen pressures and on certain catalytic systems, such as cobalt- and ruthenium-based catalysts. The rates of the secondary reactions increase exponentially with chain length. Much controversy exists whether these chain length dependencies stem from differences in physisorption, solubility or diffusivity. Preferential physisorption of longer hydrocarbons and increase of the solubility with chain length influences the product distribution and results in a decreasing olefin to paraffin ratio with increasing chain length. Process development and reactor design should be based on reliable kinetic expressions and detailed selectivity models.

2.1 Introduction

Literature on the kinetics and selectivity of the Fischer-Tropsch synthesis can be divided into two classes. Most studies aim at catalyst improvement and postulate empirical power law kinetics for the carbon monoxide and hydrogen conversion rates and assume a simple polymerization reaction following an Anderson-Schulz-Flory (ASF) distribution for the total hydrocarbon product yield. This distribution describes the entire product range by a single parameter, α, the probability of the addition of a carbon intermediate (monomer) to a chain. Relatively few kinetic studies under industrial conditions aim at understanding the reaction mechanisms. Some authors derived Langmuir-Hinshelwood-Hougen-Watson (LHHW) or Eley-Rideal type of rate expressions for the reactant consumption and proposed quantitative formulations to describe the product distribution of linear and branched paraffins and olefins, and alcohols. Models which combine the prediction of the overall consumption of the reactants with a prediction of the product distribution are very scarce in literature, despite their utmost value for understanding and modeling the FT process.

Recently, interest in the distribution of the Fischer-Tropsch products raised from improvements of the analysis of all isomers and products which can not be described with the classical ASF distribution. Also the mechanism of CO hydrogenation has remained a subject of immense controversy and uncertainty. A critical review on the various reaction mechanisms and on the kinetic relations proposed is the subject of this chapter. Areas which require further research will be defined.

2.2 Kinetic experiments

Diffusion limitation of one of the reactants results in an incomplete utilization of the catalyst particles and leads to changes in reactivity and selectivity. Zimmerman and Bukur [1] assumed first order kinetics with respect to hydrogen and proved transport limitations of H_2 to occur at particle diameters greater than 0.2 mm ($T > 235$ ˚C) with a fused iron ammonia synthesis catalyst. Post et al. [2] also used first order behavior and observed transport limitations of hydrogen at high temperatures ($T > 220$ ˚C; $d_P > 0.4$ mm) with a number of iron- and cobalt-based catalysts in a fixed bed microreactor. A common feature of these studies [1, 2] is the assumption that H_2 is the limiting reactant and the overall FT reaction rates are described as first order in H_2. Iglesia et al. [3] showed that under FT conditions CO becomes diffusion-limited. The relative transport rates of H_2 and CO within liquid-filled pores has been described by

the dimensionless quantity γ_0 [3]:

$$\gamma_0 = \frac{D_{H_2}/H_{H_2}}{D_{CO}/H_{CO}} \tag{2.1}$$

where D and H are the diffusivity coefficient and Henry coefficient, respectively. Under typical Fischer-Tropsch conditions (200 $^\circ$C, 2.1 MPa), γ_0 is about 1.9 [3–5]. Intrinsic FT kinetic measurements should be performed with small ($d_P < 0.2$ mm) catalyst particles in order to eliminate diffusion limitations of one of the reactants.

2.3 Adsorption

2.3.1 H_2 Adsorption

Hydrogen molecules react either in molecular state or via dissociative adsorption. Most transition metals are able to dissociate hydrogen on the catalyst surface [6, 7]. Heats of chemisorption of H_2 on Group VIII unsupported metals increases in the order: Co, Ni, Fe. [8, 9], see Figure 2.1. Dissociative adsorption follows the weak molecular physisorbed state of dihydrogen:

$$H_2 + 2s \rightleftarrows 2Hs \tag{2.2}$$

where s is a catalytic site.

Most adsorption studies of hydrogen are carried out on pure metals. However, Fischer-Tropsch catalysts are generally supported and promoted metals. Under FT process conditions the catalysts consist of mixtures of catalytic materials (metal, metal oxides and carbides). Dry et al. [10] measured the heats of adsorption of CO, CO_2 and H_2 on unpromoted and on K_2O-promoted reduced magnetite. The initial heat of adsorption of H_2 (80 kJ/mol) on unpromoted reduced magnetite is significantly lower than of CO (113 kJ/mol) and of H_2 on a clean iron film (about 135-150 kJ/mol) [8]. Promoters influence the bond strength of hydrogen to metal. Addition of alkali metals (usually K_2O) to iron catalysts promotes electron transfer to the iron and inhibits hydrogen adsorption, since adsorption of hydrogen induces electron donation to the iron surface [10–13].

Curtis Conner and Falconer [14] reviewed the influence of spillover in heterogeneous catalysis. Spillover proceeds by surface diffusion of adsorbed species from a surface to a different surface that does not adsorb the active species under the same conditions. Spillover of hydrogen from an oxide or a carbon surface is important

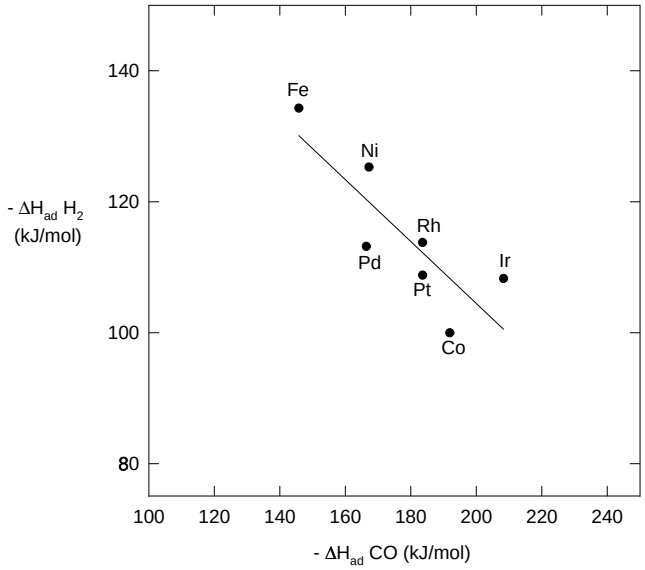

Figure 2.1 Variation of H_2 chemisorption with CO chemisorption on group VIII metals (Vannice [8]).

because the majority of the metal catalysts consists of metal particles supported on oxidic supports. Hydrogen usually dissociates on a metal surface and then spills over to the support. In this way, the catalyst support can act as a hydrogen atom reservoir [14, 15]. The influence of spilt-over hydrogen has never been quantified in kinetic rate equations of the FT synthesis, but can play a significant role.

Hydrogen reacts either in the molecular state or adsorbed dissociated state during the FTS, depending on catalyst, reaction conditions and more important co-adsorption of other species.

2.3.2 CO Adsorption

Both associative and dissociative adsorption of CO occurs. The role of CO adsorption in FTS has been discussed for a long time in literature. Reactions of dissociated CO as well as associated CO with hydrogen are reported. Therefore, adsorption measurements of CO (and H_2) on supported FT catalysts are extremely valuable for mechanistic schemes.

Dissociative adsorption of CO has been demonstrated by X-ray photo-electron spectroscopy (XPS) or pulse techniques for Ni, Co, Ru, and Fe at elevated temperatures ($T > 350$ K) [16]. Associated adsorption of CO via a carbon metal bond is the precursor state to dissociation [6, 7, 17, 18]. CO may be dissociated to a carbidic species according to:

$$\mathrm{CO} + s \rightleftarrows \mathrm{CO}s \tag{2.3}$$

$$\mathrm{CO}s + s \rightleftarrows \mathrm{C}s + \mathrm{O}s \tag{2.4}$$

At room temperature, CO adsorption is dissociative for metals more to the left of the periodic system (Cr, Mn, Fe), while other metals adsorb CO molecularly (Co, Ni, Ru). At high temperatures and pressures, CO dissociates on most transition metals [15]. Dissociation of CO occurs without activation ($\Delta E_{CO,G} < 0$) on Fe(110) according to Shustorovich [19]. However, various types of CO will be present on a catalyst (molecular, dissociative, and associative adsorbed CO) depending on process conditions [15, 20].

Figure 2.1 shows the general trend for the heats of adsorption of CO and H_2 on Group VIII unsupported metals. An increase of the adsorption strength of H_2 corresponds to a decrease of the strength of CO adsorption on the same metal. Van Santen and Neurock [21] explained the selectivity differences observed on different metals on the basis of potential energies of the CO dissociation and of the metal-carbon bond. E.g. methanol formation will easily be performed on metals such as Cu, which do not dissociate CO ($\Delta E_{CO,G}$= 163 kJ/mol [19]) and will not form any methane. On Ni, much methane is formed due to easy dissociation of CO ($\Delta E_{CO,G}$= 25 kJ/mol [19]). On Co and Fe, typical excellent Fischer-Tropsch catalysts, stronger metal-carbon bonds will lead to C_{2+} formation. Alkali promoters on iron catalysts increase the d-electron density distribution in iron and will result in an increase of CO adsorption [10–13, 20].

Above 350 K, CO is adsorbed more strongly than H_2 on group VIII metals [10, 16, 20, 22, 23]. In conclusion, in the temperature range of interest various states of CO (molecular, dissociative, and associative adsorbed CO) are present on the metal which displace hydrogen from the surface.

2.4 Fischer-Tropsch Catalysis

2.4.1 Catalysts

The most common Fischer-Tropsch catalysts are group VIII metals (Co, Ru, and Fe). Iron catalysts are commonly used, because of their low costs (see Table 2.1) in comparison to other active metals. Most early FT catalysts were prepared with precipitation techniques [24]. Novel catalyst preparation methods are sintering and fusing metal oxides with desired promoters. Alkali-promoted iron catalysts have been applied industrially for the Fischer-Tropsch synthesis during many years [25]. These catalysts have a high water gas shift activity, high selectivity to olefins and appear to be stable when synthesis gas with a high H_2/CO ratio is converted [26, 27].

Table 2.1 Relative prices of metals (March 1989) adapted from Rao et al. [25].

Metal	Price ratio
Iron	1
Cobalt	230
Nickel	250
Ruthenium	31,000
Rhodium	570,000

Cobalt catalysts give the highest yields and longest life-time and produce predominantly linear alkanes [28]. A precipitated cobalt catalyst on kieselguhr (Ruhrchemie) became the standard catalyst for commercial purposes in the second world war in Germany [29]. Disadvantages are the high costs of cobalt and low water gas shift activity. Therefore, cobalt catalysts are viable for natural-gas based Fischer-Tropsch processes for the production of middle distillates and high-molecular weight products [30–32]. Cobalt catalysts are not inhibited by water, resulting in a higher productivity at a high synthesis gas conversion [33].

Ruthenium is a very active but expensive catalyst for the Fischer-Tropsch synthesis relative to Co and Fe. At relatively low pressures ($P < 100$ bar) ruthenium produces much methane while at low temperatures and high pressures it is selective towards high molecular waxes [13, 34]. The molecular mass of polymethylene could reach one million at low temperature (100 $^{\circ}$C) and high pressure (1000-2000 bar) [34]. Vannice [35] determined the activity of group VIII metals supported on Al_2O_3 and reported a decrease in activity in the order Ru, Fe, Co, Rh, Pd, Pt, and Ir. The activities of Cr and Mo catalysts were measured at Sasol [13], but were found to be significantly lower than of iron.

2.4.2 Catalyst Pretreatment

The catalysts, synthesized in the form of a metal oxide, are subjected to an activation treatment to become active for FT synthesis. Cobalt, nickel, and ruthenium are almost always reduced in H_2 at temperatures between 473 and 723 K and remain in the metallic state under process conditions [24]. Recently, Ernst et al. [36] reported the behavior of a cobalt silica catalyst both during reduction and for Fischer-Tropsch reaction. Before reduction the cobalt is present as Co_3O_4 spinel phase. A two-step reduction by H_2 at 673 K of Co_3O_4 to CoO and to Co^0 was observed.

The pretreatment for iron is not as straightforward. The common activation treatments for iron catalysts are H_2 reduction, CO reduction or reduction in synthesis gas (induction). Reduction of Fe_3O_4 by hydrogen to the zero-valent state is reported by, for example, Rao et al. [37] and Bukur et al. [38]. Lox et al. [39] reported that H_2 reduction at 220 ˚C results in 20 % metallic iron. After pretreatment of Fe-SiO_2 with CO or synthesis gas, the χ-carbide is the dominant iron phase [37, 38, 40, 41]. Pretreatment with synthesis may also result in formation of ε'-carbide [40]. More details on the composition and catalytic activity of the different iron phases is given below.

Iron catalysts are often promoted with Cu, which increase the rate of reduction enabling a lower reduction temperature [12, 13, 24]. Bukur et al. [38, 42–45] studied several reducing gases (CO, H_2 and H_2/CO=0.68) in a fixed bed and concluded that activation in CO (at 280 ˚C and 1 bar for 24 h) led to catalysts with higher initial activity and better selectivity towards higher hydrocarbons than H_2-activated catalysts. Shroff et al. [46] determined the effect of activation conditions on catalyst behavior. They also studied the micro-structure of the catalyst by electron microscopy and other bulk and surface characterization techniques. They observed that magnetite crystals transform to smaller carbide crystallites. Deposition of carbon on these crystallites causes further segregation of the particles.

2.4.3 Fischer-Tropsch Activity

Cobalt, nickel, and ruthenium remain in the metallic state under FT conditions [24]. Ernst et al. [36] concluded that a completely reduced cobalt remains in the metallic state during CO/H_2 reaction by in situ EXAFS (extended X-ray absorption fine structure).

The composition of iron-based catalysts changes during Fischer-Tropsch synthesis. Characterization of the several phases with *in situ* laser Raman spectroscopy [47], *in situ* magnetic measurements [48] or Mössbauer spectroscopy [37, 48] may give ev-

idence of the reactivity of the several active species. Several phases of iron are known in iron-based catalysts subjected to FT synthesis conditions. These include metallic iron (α-Fe), iron oxides (hematite, α-Fe_2O_3; magnetite Fe_3O_4, and Fe_xO), and five different forms of iron carbides O-carbides (carbides with carbon atoms in octahedral interstices, ε-Fe_2C, ε'-$Fe_{2.2}$ C, and Fe_xC), and TP-carbides (carbides with carbon atoms in trigonal prismatic interstices, χ-$Fe_{2.5}C$ and Fe_3C) [13, 37, 39, 46, 47]. The formation and composition of these iron phases depends on the process conditions, catalyst deactivation and catalyst composition. The catalytic activity of each of these phases with respect to the Fischer-Tropsch reaction is still controversial [13, 44, 46].

There are a number of studies on iron catalysts concerning the role of iron phases in FT synthesis. Raupp and Delgass [49] and Niemantsverdriet et al. [50] proposed that iron carbide formation is needed for a high FT activity. Based on X-ray diffraction, Dictor and Bell [51] concluded that a mixture of χ- and ε'-carbides are the active phase on iron catalysts. Bukur et al. [44] showed with Mössbauer spectroscopy that the FT activity of H_2-activated catalysts coincided with the conversion of metallic iron to ε'-carbide. They concluded that the active phase of CO-pretreated catalyst was the χ-carbide [44].

Zhang and Schrader [47] concluded that two active sites operated simultaneously on the surface of iron catalysts: Fe^0/Fe-carbides and Fe-oxide (Fe_3O_4). The carbide phase is active towards dissociation of CO and formation of hydrocarbons, while the oxide phase adsorbs CO associatively and produces predominantly oxygenated products. Lox et al. [39] and Shroff et al. [46] concluded that the magnetite phase has negligible catalytic activity towards FT reactions whereas carbide formation resulted in a high FT activity. Several studies have shown that the ε'-carbide phase is the active form for CO hydrogenation on iron catalysts [49, 50, 52]. More recent studies show that the χ-carbide can also be the active phase for the FT synthesis [37, 44, 53].

2.4.4 Water Gas Shift Activity

Cobalt and ruthenium catalysts are not very active towards the WGS reaction in contrast to most iron-based Fischer-Tropsch catalysts [54]. The water gas shift (WGS) reaction is important when synthesis gas with non-stoichiometric amounts of hydrogen is used. The WGS reaction is an equilibrium reaction and may reach equilibrium at high temperatures ($T > 250$ $^\circ$C) on catalysts with a high water gas shift activity [55, 56]. Several authors proposed that magnetite (Fe_3O_4) is the most active phase for the WGS reaction [37, 47, 54, 57, 58] on iron catalysts. Rao et al. [37] studied the

iron phase of Fe/Cu/K/SiO_2 catalysts from the demonstration unit at LaPorte, Texas (August, 1992) with Mössbauer spectroscopy. The changes of the magnetite phase corresponded to the WGS reaction activity during time-on-stream. Lox et al. [39] showed that Fe_3O_4 coexists with various iron carbides on the catalyst during synthesis gas reactions. It is generally assumed that the WGS reaction and the FT reaction proceed on different active sites.

2.5 Mechanism

2.5.1 Fischer-Tropsch Synthesis

The mechanism of the hydrocarbon and oxygenate formation in the FTS has been reviewed by several authors [13, 16, 18, 24, 59]. Recent reviews are given by Hindermann et al. [60], Dry [61], Dry [62], and Adesina [63]. Here we give a summary of the mechanisms for the formation of linear hydrocarbons which are supported by experiments. The FTS is a polymerization reaction with the following steps [63]: 1. reactant adsorption; 2. chain initiation; 3. chain growth; 4. chain termination; 5. product desorption; 6. readsorption and further reaction.

A variety of surface species were proposed to describe chain initiation and chain growth. Figure 2.2, adapted from Schulz et al. [64] and Rofer-De Poorter [7], gives an overview of observed and postulated species on the catalyst surface during Fischer-Tropsch synthesis. Reactants: **1,2,3,4,5**; oxygen containing intermediates: **6,7,8** and hydrocarbon intermediates: **9,10,11,12**. Several compounds are possible monomers for chain growth.

The most important growth mechanism for the hydrocarbon formation on cobalt [28], iron [51, 65], and ruthenium catalysts [65, 66] is the surface carbide mechanism by CH_2 insertion [13, 22, 67, 68]. Figure 2.3 shows a schematic representation of the initiation, growth and termination of chains according to this mechanism. The monomer of the carbide mechanism is a methylene (CH_2) species (see Figure 2.2: nr. **10**). CO and H_2 are assumed to adsorb dissociatively. Several species like CH (**9**), CH_2 (**10**) and CH_3 (**11**) can be formed this way. Chain growth occurs by insertion of the monomer in a growing alkyl species (**12**). Termination can take place by abstraction of hydrogen to an olefin or addition of a CH_3 species (**11**) or hydrogen to form a paraffin. The presence of methylene has been identified with use of isotopic-tracer techniques on Ru/SiO_2 [69], on unsupported Co, Ni/SiO_2, and Ru/Al_2O_3 [65, 70] and on Fe/Al_2O_3 [71]. Several authors mentioned a mechanism where CH_2 is formed by hydrogen assisted CO dissociation [11, 22, 72]. Undissociated adsorbed CO re-

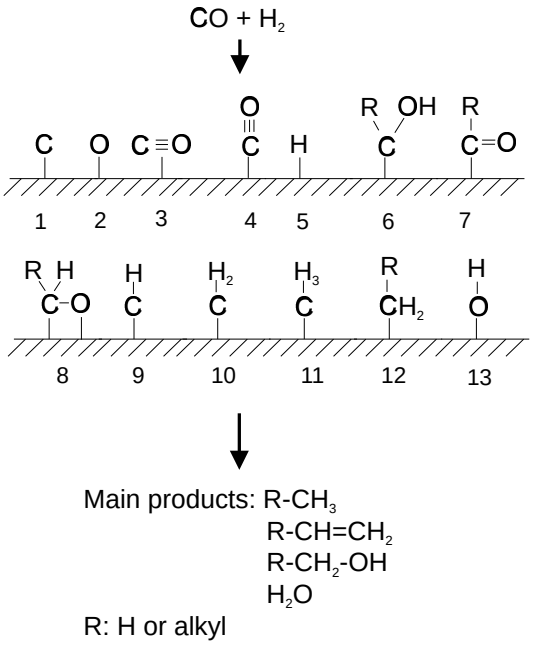

Figure 2.2 Observed and postulated chemisorbed species during Fischer-Tropsch synthesis (adapted from Schulz et al. [64]).

acts with hydrogen before the CH_2 species is formed. After that, the enolic (HCOH) species is dissociated in water and a methylene species, while chain growth proceeds in a similar way.

The carbide mechanism by CH_2 insertion is the most plausible mechanism for the hydrocarbon formation reactions on ruthenium, cobalt, and iron. It is uncertain if the monomer formation proceeds via hydrogenation of dissociated or undissociated CO. The set of elementary reactions proposed for the formation of linear hydrocarbons is given in Table 2.2 [18, 22, 75, 76].

Secondary reactions occur when primary products desorb from a site and interact with another catalytic site before leaving the reactor. Novak et al. [77, 78] listed possible secondary reactions of α-olefins: (i) hydrogenation to give n-paraffins, (ii) isomerization, (iii) cracking and hydrogenolysis, (iv) insertion into growing chains, mostly effective for C_2 H_4 and C_3 H_6, and (v) readsorption and initiation of hydrocarbon chains. Schulz et al. [68, 74] showed a possible reaction mechanism for the readsorption of olefins followed by hydrogenation to paraffins or isomerization to internal olefins via double bond shift reactions (Figure 2.4). Secondary reactions can influence the type and molecular weight of the hydrocarbon products as will be proved later.

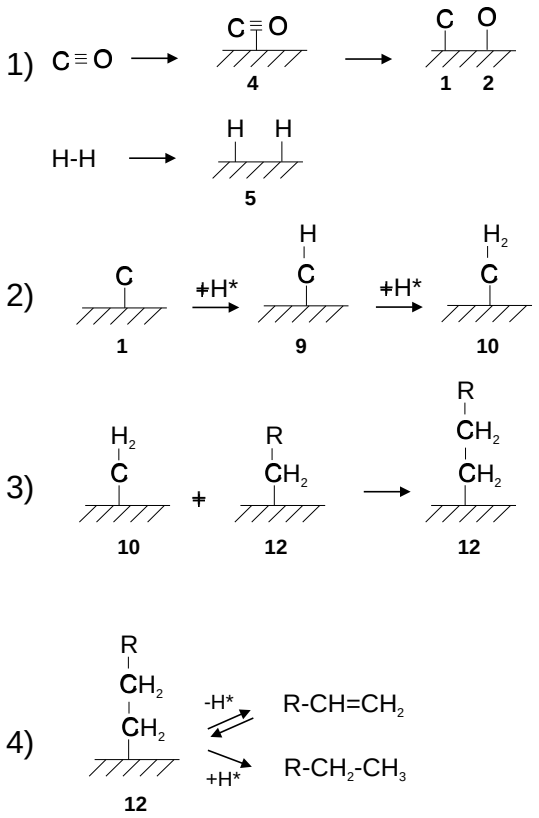

Figure 2.3 Carbide mechanism for the Fischer-Tropsch synthesis [18, 73].

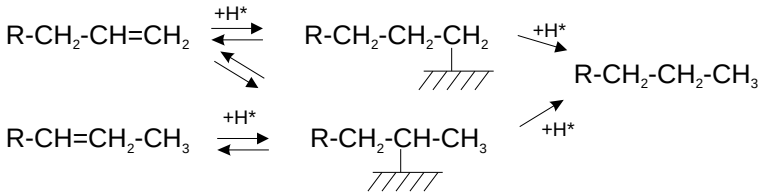

Figure 2.4 Secondary reactions of olefins (Schulz et al. [74]).

Table 2.2 Proposed mechanism of the hydrocarbon synthesis from CO and H_2 [18, 22, 75, 76].

Adsorption	
1	$CO + s \rightleftarrows COs$
2	$COs + s \rightleftarrows Cs + Os$
3	$H_2 + 2s \rightleftarrows 2Hs$
Surface reactions	
Water formation	
4	$Os + Hs \rightarrow HOs + s$
5	$HOs + Hs \rightarrow H_2O + 2s$
or	$Os + H_2 \rightarrow H_2O + s$
Chain initiation	
6	$Cs + Hs \rightleftarrows CHs + s$
7	$CHs + Hs \rightleftarrows CH_2s + s$
8	$CH_2s + Hs \rightleftarrows CH_3s + s$
or	$COs + H_2 \rightleftarrows CHOHs$
	$CHOHs + H_2 \rightleftarrows CH_2s + H_2O$
Methanation	
9	$CH_3s + Hs \rightarrow CH_4 + s$
Chain growth	
10	$C_nH_{2n+1}s + CH_2s \rightarrow C_{n+1}H_{2n+3}s + s$
Hydrogenation to paraffins	
11	$C_nH_{2n+1}s + Hs \rightarrow C_nH_{2n+2} + 2s$
β-dehydrogenation to olefins	
12	$C_nH_{2n+1}s \rightleftarrows C_nH_{2n} + Hs$

2.5.2 Water Gas Shift Reaction

Several mechanisms for the water gas shift reaction are proposed in the literature. Single studies of the water gas shift reaction over supported iron and cobalt shift catalysts suggest the appearance of formate species [54]. A mechanism based on a reactive formate intermediate is shown in Figure 2.5 [58, 75, 79–82]. The formate species can be formed by the reaction between a hydroxy species or water and carbon monoxide in the gas phase or in the adsorbed state. The hydroxy intermediate can be formed by the decomposition of water. The formate intermediate is reduced to adsorbed or gaseous carbon dioxide. Rofer-De Poorter [7] suggested that a mechanism with direct oxidation of adsorbed or gas-phase CO to CO_2 [58, 83–87], presented in Figure 2.6, is more plausible in conjunction with the Fischer-Tropsch synthesis on iron catalysts. The oxygen intermediate can be formed from the dissociation of water. Direct oxidation of CO proceeds via a regenerate or redox mechanism where H_2O oxidizes the surface with formation of H_2, and CO subsequently reduces the surface with the formation of CO_2 [58]. Rethwisch and Dumesic [58] studied the water gas shift reaction on several supported and unsupported iron oxide and zinc oxide catalysts. They suggested that the WGS reaction over unsupported magnetite proceeds via a direct oxidation mechanism, while all supported iron catalysts operate via a mechanism with formate species due to limited change of oxidation state of the iron cations. From the above considerations, we conclude that the water gas shift reaction on supported iron catalysts during the FTS proceeds on the magnetite phase (see before) by reaction of undissociated CO via a formate intermediate.

2.6 Selectivity of the Fischer-Tropsch Synthesis

2.6.1 Introduction

The products from the FTS on Co, Fe, and Ru show the following characteristics [22, 32, 59]:

1. The carbon-number distributions for hydrocarbons gives the highest concentration for C_1 and decreases monotonically for higher carbon numbers, though around C_3-C_4 often a local maximum is observed. Examples of these distributions for iron [88], cobalt [89] and ruthenium catalysts [32] are plotted in Figure 2.7.

2. Monomethyl-substituted hydrocarbons are present in moderate amounts while

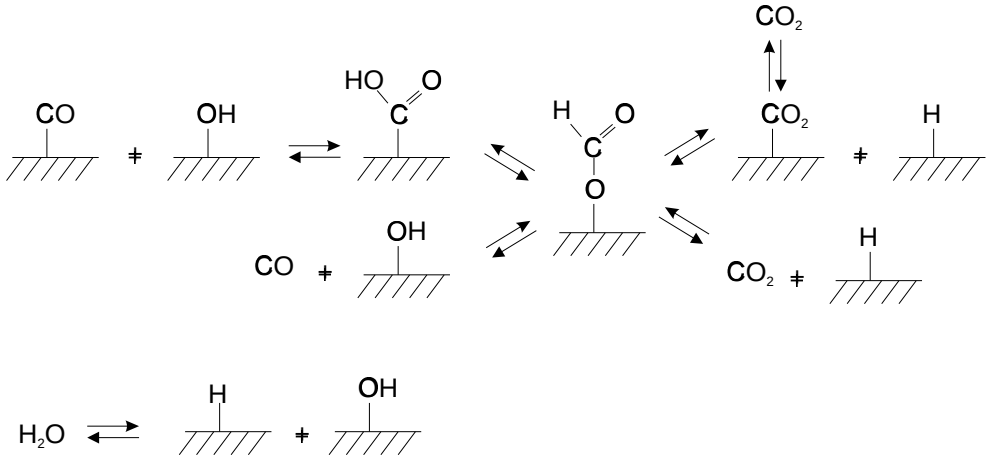

Figure 2.5 Water gas shift reaction mechanism via formate species (Lox and Froment [75]).

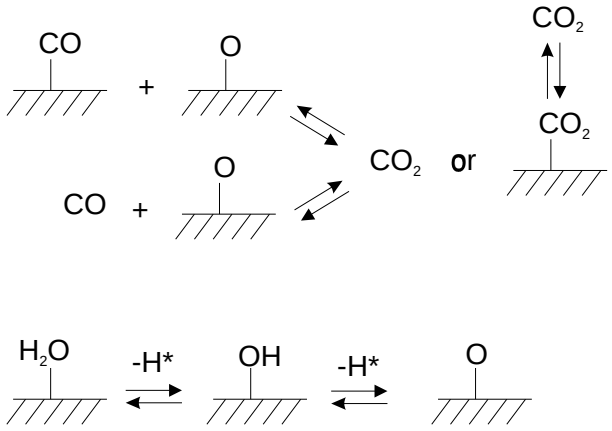

Figure 2.6 Water gas shift mechanism via direct oxidation (Lox and Froment [75]).

dimethyl products are present in significantly smaller amounts than monomethyl. None of these branched products contain quaternary carbon atoms on Co, Fe, and Ru [59].

3. Olefins from iron catalysts exceed 50% of the hydrocarbon products at low carbon numbers, and more than 60% of these are α-olefins. The ethene selectivity is low in comparison to propene. The olefin content decreases asymptotically to zero with increasing carbon number on Co, Ru, and Fe catalysts. For cobalt catalysts both the fraction of total olefins and α-olefins are smaller, and both decrease with carbon number (see Figure 2.8).

4. A change in chain growth parameter in the distribution is only observed for linear paraffins and not for olefins (see Figure 2.9).

5. Yields of alcohols are maximal at C_2 and decrease with carbon number. Low yields of methanol are probably the result of thermodynamic limitations (see Figure 2.9).

2.6.2 Influence of Process Conditions on the Selectivity

The process conditions as well as the catalyst influence the product selectivity. The effect of temperature, partial pressures of H_2 and CO, time on stream, composition and reduction of the catalyst will be discussed briefly. Table 2.3 shows the general influence of different parameters on the selectivity. The effect of the reactor temperature as well as the hydrogen to carbon monoxide ratio on the chain growth probability factor will be described in more detail in the next chapter. The influence of the synthesis gas conversion on the product selectivity is strongly related to the influence of the process conditions (see also paragraph on the influence of space velocity). Donnelly and Satterfield [90] and Dictor and Bell [51] reported that the chain growth factor was insensitive to conversion over a wide range.

Temperature

Increase of temperature results in a shift towards products with a lower carbon number on iron [51, 90], ruthenium [13], and cobalt [13] catalysts. Donnelly and Satterfield [90], Dictor and Bell [51], and Anderson [24] observed an increase of the olefin to

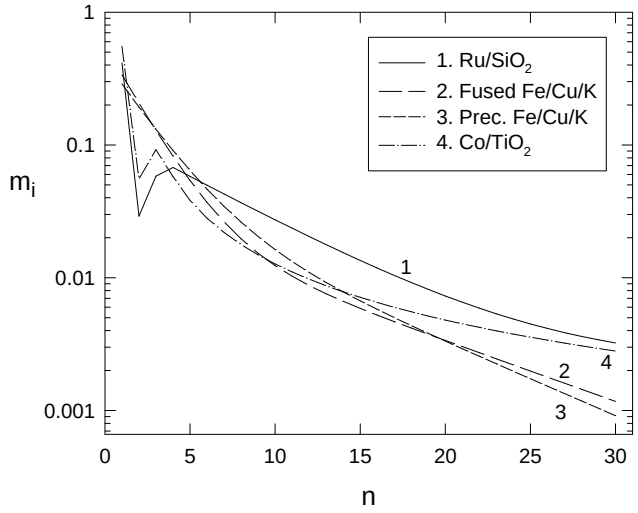

Figure 2.7 Total hydrocarbon selectivity on Co/TiO_2 (T= 473 K, H_2/CO= 2.1, P= 2.0 MPa, data from Iglesia et al. [89]), Ru/SiO_2 (T= 485 K, H_2/CO= 2, P= 0.51 MPa, data from Madon et al. [32]), and fused and precipitated Fe/Cu/K (data from Donnelly et al. [88]).

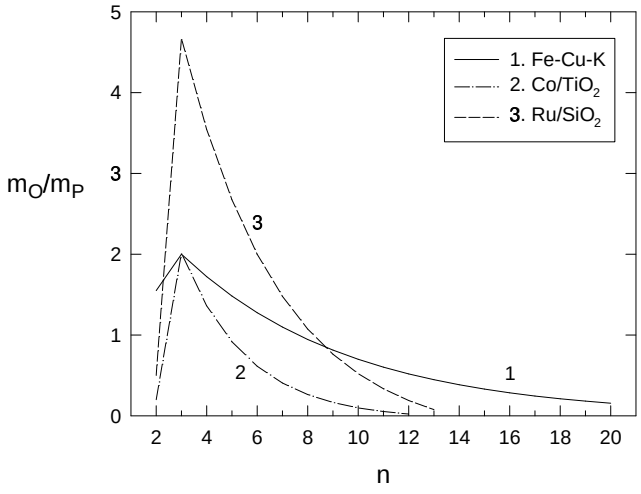

Figure 2.8 Olefin to paraffin ratio on Co/TiO_2 (T= 473 K, H_2/CO= 2.1, P= 2.0 MPa, data from Iglesia et al. [89]), Ru/SiO_2 (T= 485 K, P= 0.51 MPa, H_2/CO= 2, data from Madon et al. [32]), and precipitated Fe/Cu/K (T= 489 K, P= 1.62 MPa, H_2/CO= 2, data from Madon et al. [32])

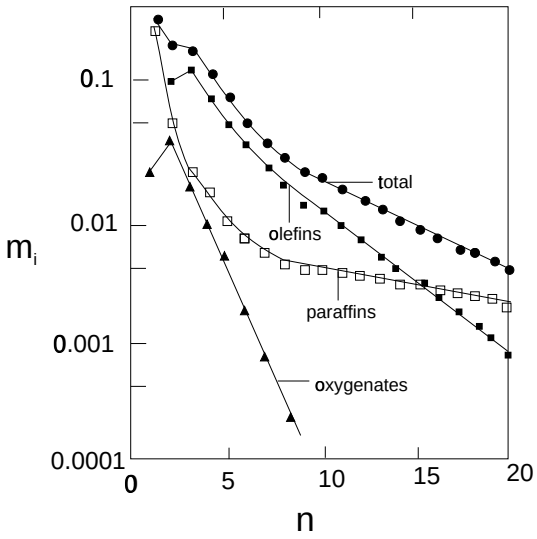

Figure 2.9 Overall product distribution on precipitated Fe/Cu/K catalyst, H_2/CO= 0.7, T= 263 ˚C, P= 2.4 MPa (from Donnelly and Satterfield [90]).

paraffin ratio on potassium-promoted precipitated iron catalysts with increasing temperature. However, Dictor and Bell [51] reported a decrease of the olefin selectivity with increasing temperature for unalkalized iron oxide powders.

Partial pressure of H_2 and CO

Most studies show that the product selectivity shifts to heavier products and to more oxygenates with increasing total pressure [13]. Increasing H_2/CO ratios in the reactor result in lighter hydrocarbons and a lower olefin content [51, 90]. Donnelly and Satterfield [90] observed a decrease of the olefin to paraffin ratio from 6 to 1 by increasing the H_2/CO ratio from 0.3 to 4. Dry [13] proved a relation between the methane selectivity and the factor $P_{H_2}^{1/2}/(P_{CO} + P_{CO_2})$ for alkaline-promoted fused iron catalysts in a fluidized bed reactor. This indicates that CO_2 appears to play an important role. Increasing CO_2 pressures result in a decrease of the methane selectivity.

Space velocity

The influence of the space velocity of the synthesis gas (residence time) on the selectivity has been investigated [91–93]. Increase of the olefin to paraffin ratio with increasing space velocity (thus a decrease of the conversion) was observed by Kuipers

Table 2.3 Selectivity control in Fischer-Tropsch synthesis by process conditions and catalyst modifications (from Röper [12]).

Parameter	Chain length	Chain branching	Olefin select.	Alcohol select.	Carbon deposition	Methane select.
Temperature	↓	↑	∗	↓	↑	↑
Pressure	↑	↓	∗	↑	∗	↓
H_2/CO	↓	↑	↓	↓	↓	↑
Conversion	∗	∗	↓	↓	↑	↑
Space velocity	∗	∗	↑	↑	∗	↓
Alkali content iron catalyst	↑	↓	↑	↑	↑	↓

Increase with increasing parameter: ↑
Decrease with increasing parameter: ↓
Complex relation: ∗

et al. [92] on a poly-crystalline cobalt foil (Goodfellow, 99.9 % purity, thickness 0.25 mm), Bukur et al. [91] on a commercial (Ruhrchemie) supported iron catalyst (Fe/Cu/K/SiO_2), and Iglesia et al. [93] on TiO_2-supported ruthenium catalysts. Bukur et al. [91] measured no effect of the space velocity on the molecular weight of the hydrocarbons, while Iglesia et al. [93] observed an increase of the average molecular weight of the products with decrease of the space velocity. The selectivity to methane and olefins decreases with a decrease of the space velocity, while the selectivity towards paraffins remains unchanged (see Figure 2.10, obtained from Iglesia et al. [3]). The effect of the space velocity on the secondary reactions of olefins will be discussed more detailed below.

Time on stream

Deactivation of catalysts during the FTS may affect the activity and selectivity to hydrocarbon products. Increase of the selectivity to oxygenates is reported by Donnelly and Satterfield [90] after a period of 1300 hours time on stream with a precipitated

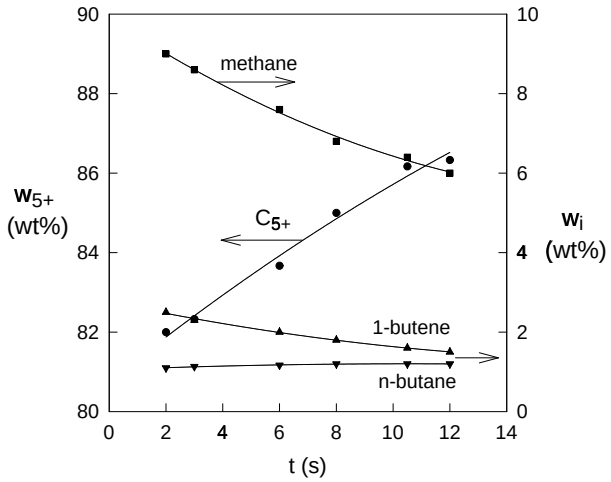

Figure 2.10 Residence time effect on methane, C_{5+}, n-butane, and 1-butene selectivity on Co/TiO_2 (473 K, 2.0 MPa, H_2/CO= 2.1, 9.5-72 % CO conversion [3]).

promoted iron catalyst. An increase of the methane selectivity and low-molecular products is observed on iron catalysts [90, 91, 94]. It is known that selectivity changes with time can be caused by the formation of carbonaceous deposits on sites with potassium promoters [13]. Dry [13] showed that these deposits can be removed from a fused iron catalyst by hydrogen treatment at temperatures higher than 350 ˚C. Sintering of precipitated iron catalysts lead to reduction of the surface area from 300 m^2/g for a fresh catalyst to about 90 m^2/g for a used catalyst [13, 39, 44]. Agglomeration of initially small crystallites is enhanced by high water pressures.

Reduction of the catalyst

Bukur and co-workers studied the effect of pretreatment conditions of promoted iron catalysts on the hydrocarbon selectivity and activity [38, 42–45]. The hydrocarbon selectivity appeared to relate strongly on the pretreatment procedure. Figure 2.11 shows the effect of pretreatment on the hydrocarbon selectivity [38]. Low methane and C_2-C_4 selectivities and high diesel fuel and wax (C_{12+}) selectivities were observed at pretreatments with CO and CO/H_2. The figure also shows the influence of reduction temperature with H_2 pretreatment. Reduction at 280 ˚C causes a shift to products with higher carbon number relative to 250 ˚C. Olefin selectivities are reported to decrease after hydrogen reduction in comparison to reduction with CO or synthesis gas.

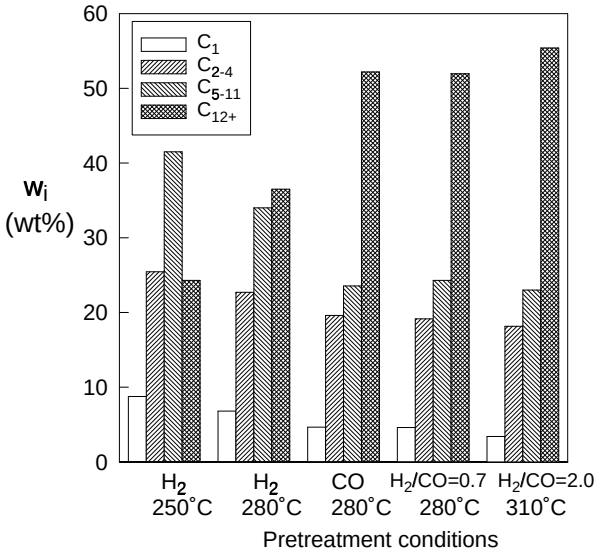

Figure 2.11 Effect of pretreatment conditions on the hydrocarbon selectivity at 250 ˚C, 1.48 MPa, H_2/CO= 0.67, 5.5 10^{-4} Nm^3 kg_{cat}^{-1} s^{-1} from Bukur et al. [38].

2.7 Product Selectivity Models

2.7.1 Anderson-Schulz-Flory Distribution

According to Anderson [24] the distribution for n-paraffins can be described by the Anderson-Schulz-Flory (ASF) equation:

$$m_n = (1-\alpha)\alpha^{n-1}, \quad \frac{w_n}{n} = \frac{(1-\alpha)^2}{\alpha}\alpha^n \tag{2.5}$$

where the growth probability factor α is independent of n and m_n is the mole fraction of a hydrocarbon with chain length n. α is defined by:

$$\alpha = \frac{R_p}{R_p + R_t} \tag{2.6}$$

where R_p and R_t are the rate of propagation and termination, respectively. α determines the total carbon number distribution of the FT products, see Figure 2.12. The range of α is dependent on the reaction conditions and catalyst type. Dry [95]

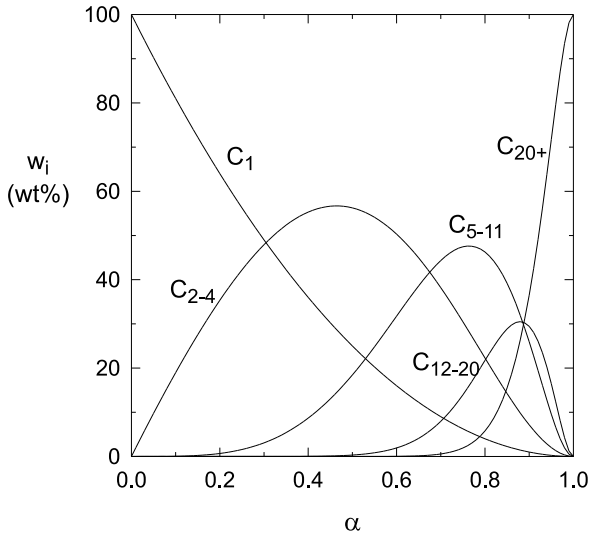

Figure 2.12 Hydrocarbon selectivity as function of the chain growth probability factor α, calculated with eq 2.5.

reported typical ranges of α on Ru, Co, and Fe of: 0.85-0.95, 0.70-0.80, and 0.50-0.70, respectively. The effect of the reactor temperature is shown in Figure 2.13. The chain growth probability, α, decreases with an increase of the reactor temperature [51, 57, 90, 95, 96]. A large variation in α is observed at temperatures higher than 280 $^{\circ}$C [57, 95, 96]. Figure 2.14 shows that the values of α depend on the H_2/CO ratio in the reactor. It must be noted that reported values of α from Lox and Froment [57] and Dictor and Bell [51] were obtained with a constant partial pressure of H_2 and a varying CO pressure. The data of Dictor and Bell [51] on a Fe_2O_3/K catalyst depend very little on the H_2/CO ratio in contrast to other studies on Fe, Fe/Cu/K, and Ru catalysts. A decrease of α is observed at higher H_2/CO ratios [18, 51, 57, 90].

Figure 2.15a shows the growing mechanism for a constant α. The ASF equation does not distinguish between different product types. A semi-logarithmic plot of the mole fraction against carbon number yields the well-known Schulz-Flory diagram (fig. 2.16a), where the slope of the straight line yields the chain growth probability α.

In practice, a multicomponent product mixture is formed. Main products are paraffins and olefins. Dependent on process conditions and catalysts, oxygenated prod-

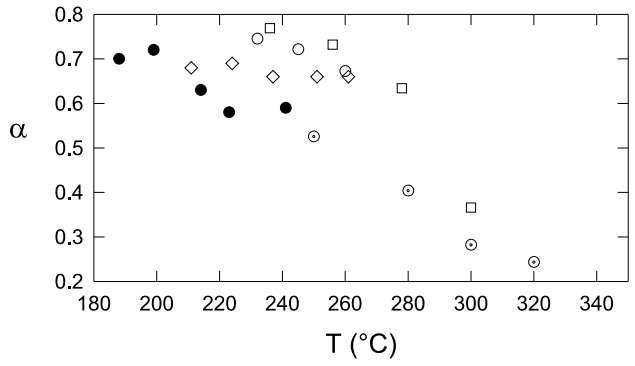

Figure 2.13 Chain growth probability factor as a function of temperature. ○: Fe/Cu/K commercial Ruhrchemie catalyst, gas-slurry system, $(H_2/CO)_{feed}$= 0.7, 2.72 MPa, 0.33 10^{-4} Nm^3 $kg^{-1}s^{-1}$ [90]; ●: Fe_2O_3 catalyst, gas-solid system, $(H_2/CO)_{feed}$= 3, 0.8 MPa [51]; ◇: Fe_2O_3/K catalyst, gas-solid system, $(H_2/CO)_{feed}$= 3, 0.8 MPa [51]; □: Ru catalyst, gas-solid system, $(H_2/CO)_{feed}$= 3, 0.8 MPa [95, 96]; ⊙: Fe/Cu/K commercial Ruhrchemie catalyst, gas-solid system, $(H_2/CO)_{feed}$= 3, 2.0 MPa, [57].

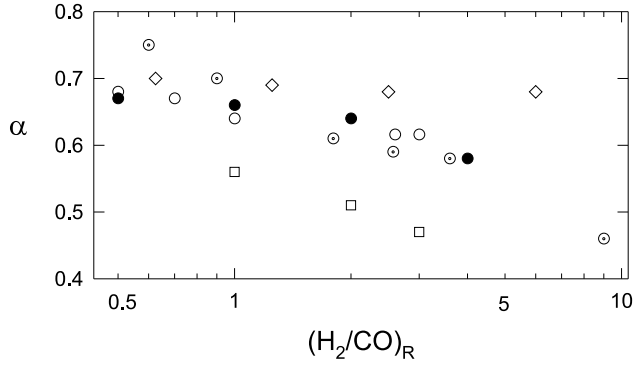

Figure 2.14 Chain growth probability factor as a function of hydrogen to carbon monoxide ratio. ○: Fe/Cu/K catalyst, gas-slurry system, 1.48 MPa, 260 ˚C [90]; ●: Fe_2O_3 catalyst, 212 ˚C , gas-solid system, 0.5 -1.2 MPa [51]; ◇: Fe_2O_3/K catalyst, 240 ˚C, gas-solid system, 0.8 MPa, [51]; □: Ru catalyst, 275 ˚C, gas-solid system, 0.8 MPa [18]; ⊙: Fe/Cu/K commercial Ruhrchemie catalyst, gas-solid system, 250 ˚C , 1.0 - 2.5 MPa [57].

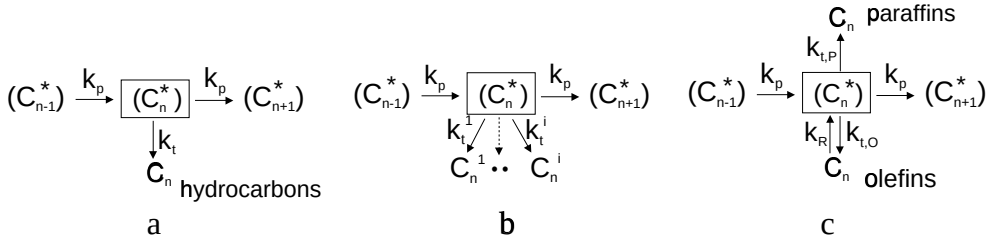

Figure 2.15 Reaction growth schemes Fischer-Tropsch synthesis from Glebov and Kliger [97]. a. Classical Anderson-Schulz-Flory model with one termination constant for all products. b. Multiple termination probabilities originating from a single intermediate. c. Termination to paraffins and olefins, whereas the latter can be readsorbed on the catalytic surface.

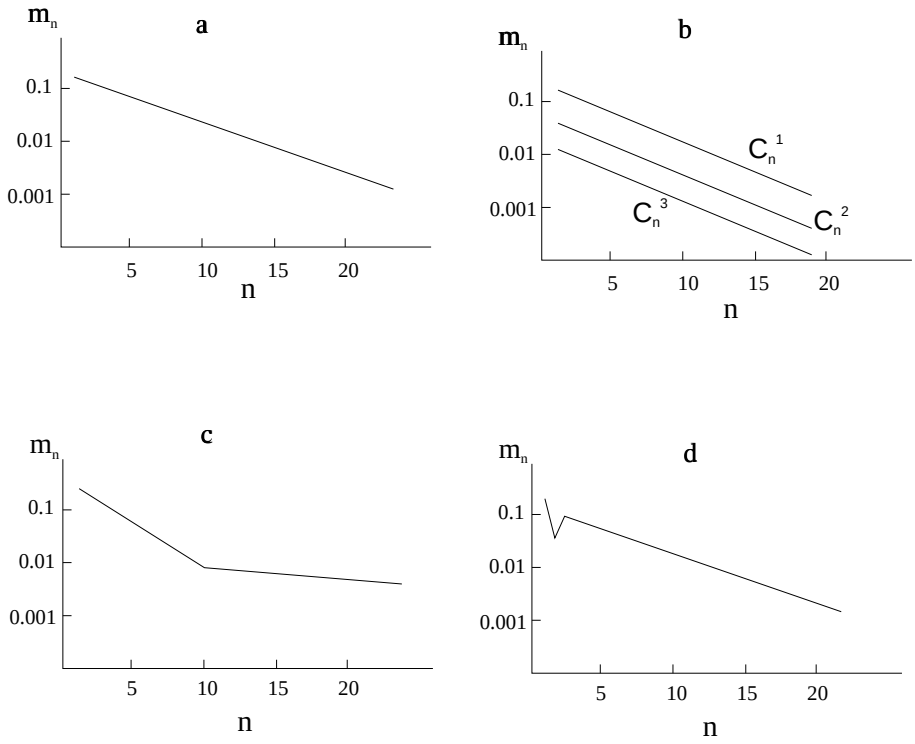

Figure 2.16 Schematic product distribution graphs of the Fischer-Tropsch hydrocarbons from Glebov and Kliger [97]. a. Classical Anderson-Schulz-Flory distribution of all products. b. Multiple termination probabilities yield several parallel straight distributions. c. Distribution graph with two different chain growth probabilities. d. Classical distribution with anomalies at C_1 and C_2 products.

ucts (for-example alcohols, aldehydes), branched hydrocarbons, and β-olefins can be formed as well. Glebov and Kliger [97] showed that the original Anderson-Schulz-Flory equation (eq 2.5) can be modified for the description of multicomponent FT products. Figure 2.15b shows the reaction scheme for this model, while the ASF diagram is presented in Figure 2.16b. Glebov and Kliger [97] assumed all products to be formed from the same intermediate. The mole fraction of a product, component type (paraffins, olefins, alcohols, and so forth) i with carbon number n can be calculated from:

$$\sum^{i} m_n^i = (1-\alpha)\alpha^{n-1} \tag{2.7}$$

with α:

$$\alpha = \frac{k_p}{k_p + \sum_i k_t^i} \tag{2.8}$$

Because Glebov and Kliger [97] assume α to be the same for the different product types, a semi-logarithmic plot of the mole fractions against carbon number show straight parallel lines (see Figure 2.16b). However, most product distributions show lines with varying slopes (see Figure 2.7) and more comprehensive models are necessary to describe these deviations from the simplified ASF distribution.

2.7.2 Deviations from ASF Distribution

2.7.2.1 Introduction

Significant deviations from the Anderson-Schulz-Flory distribution are reported in literature. The deviations were sometimes assigned to analytical difficulties [98] and non-steady state conditions of the reactor system [99]. Both effects are still important potential sources of artifacts, however, novel analytical techniques usually rule out these explanations as the major source for the observed deviations. More fundamental explanations will be discussed below.

Relatively high yield of methane

Several mechanisms have been proposed to explain the experimentally observed (see Figure 2.7) relatively high methane contents. Wojciechowski [22] and Sarup and Wojciechowski [100] modeled the distribution of linear and branched paraffins with the

use of termination probabilities. This way, the excess methane yield was described with a separate parameter for the increased termination probability of C_1 precursors. The methane termination probability parameter appears to be between 5 to 20 times larger than the termination probability to paraffins [100].

Schulz et al. [68] assumed a different catalytic site for the methanation reaction for the description of excessive methane formation on a cobalt catalyst in a slurry reactor. The authors did not specify the exact nature of these sites.

Heat and mass transfer limitations are reported in literature as possible reasons for high methane yields. Dry [95] reported that mass transfer limitations will result in an increase of the thermodynamically favored products, that is methane. The existence of hot spots, due to high reaction heats, may result in a decrease of the chain growth parameter and a higher yield of methane [51, 95].

Secondary hydrogenolysis by demethylation which may occur on FT catalysts [92, 101]:

$$C_nH^*_{2n+1} + H^* \rightarrow C_{n-1}H_{2n-1} + CH^*_3 \tag{2.9}$$

Kuipers et al. [92] modeled the hydrogenolysis of paraffins on Co catalysts. However, hydrogenolysis decreases strongly with increasing CO and H_2O pressures [93] and for reactor temperatures lower than 275 °C.

On common FT-catalysts it is difficult to point at one process responsible for the increased methane production under all circumstances. Under the absence of mass and heat transfer limitations and common H_2/CO ratios and reactor temperatures, the increased methane yield is most probably due to increased surface mobility of the methane precursor [22, 100]. Furthermore, several active sites present on most FT catalysts may result in a site which favors methane formation in comparison to chain growth [16, 68].

Anomalies of ethane and ethene (Figure 2.7)

In agreement with deviations for methane, Wojciechowski [22] used a higher surface mobility or reactivity of C_2 precursors to predict the increased production of ethane. Dependent on the reaction conditions, the termination probability to ethane is 0.5 to 2 times the value to paraffins [100].

Secondary reactions are often reported as the most possible reason for the anomalies of C_2 products: i) incorporation of ethene in growing chains [77, 78], ii) rapid readsorption of ethene [93, 101, 102]. iii) hydrogenolysis of ethene [101], and iv)

hydrogenation of ethene to ethane [92, 102, 103]. If ethene is used as monomer or building block during the FTS, an oscillating product distribution should be observed with maxima at even carbon numbers. However, such behavior has not been observed [97]. Therefore, it is not plausible that ethene is used as a building block. Secondary reactions will be discussed in more detail below. Readsorption of ethene will result in a decrease of the ethene yield and increase of ethane and higher hydrocarbons. Komaya and Bell [101] modeled the elementary reactions in FTS over a Ru/TiO_2 catalyst. Ethene could be hydrogenolyzed to methyl and methylene (monomer), with the readsorption constant of ethene approximately four orders of magnitude larger than higher olefins. Iglesia et al. [93] showed that ethene and propene obtain a higher reactivity and larger readsorption constant (factor 10) than other olefins. Secondary hydrogenation can be important over Co and Ru catalysts at high H_2/CO ratios in the reactor and a low H_2O pressure [102, 103].

Change in chain growth parameter α_n (Figure 2.7 and 2.9) and exponential decrease of the olefin to paraffin ratio (Figure 2.8)

At a carbon number of about 10, the slope of the semi-logarithmic mole fractions of hydrocarbons against carbon number increases. This phenomenon has been observed on iron [32, 51, 72, 104, 105], cobalt [22, 32, 100, 106], and ruthenium catalysts [32, 107, 108]. Suggestions for the increased chain growth parameter or two probabilities of chain growth are the occurrence of different catalytic sites [51, 109, 110] or the existence of different chain termination reactions [22, 100]. Several attempts to model the hydrocarbon distribution with two different values of α have been reported. However, analysis of detailed product distributions shows that the distribution of paraffins are curved instead of the linear distribution of olefins, [90, 91, 106]. Furthermore, the assumption of multiple catalytic sites cannot explain the decrease of the O/P ratio with increasing chain length, decreasing space velocity and increasing H_2/CO ratios in the reactor.

An example of the variation of the chain growth probability, α_n, with chain length is given in Figure 2.17 for several catalysts [32, 88, 93]. Except for carbon number two, the chain growth probability increases to a maximum value. The initial value of α is low for iron catalysts. The asymptotical value of α is between 0.85 and 0.92 in Figure 2.17.

It is widely considered that the occurrence of secondary reactions (hydrogenation, reinsertion, hydrogenolysis, isomerization) gives the most reasonable explana-

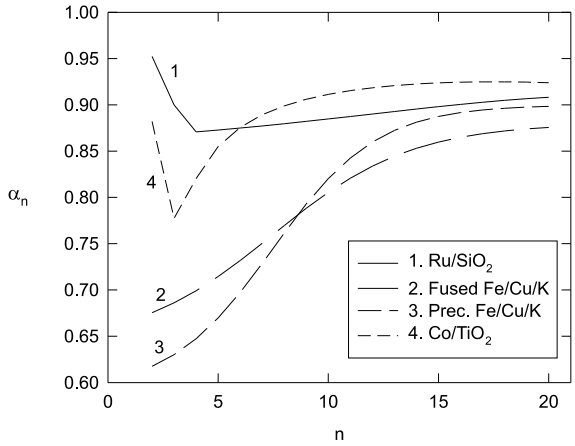

Figure 2.17 Chain growth probability factor (α_n) as function of chain length n, data from Madon et al. [32] (Ru/SiO_2, and Co/TiO_2) and Donnelly et al. [88] (fused and precipitated Fe/Cu/K).

tion for these deviations of the ASF distribution [78, 89, 92, 103, 111]. If a product is terminated by a reaction on an FT growth site to a paraffin or olefin it is called a primary product. Readsorption of olefins on growth sites may also lead to primary products whereas adsorption on other sites will produce secondary products due to hydrogenation or isomerization reactions. Secondary reactions as well as readsorption are directly influenced by space velocity. It is generally accepted that secondary reactions of olefins depend on the chain length, resulting in a decrease of the (O_n/P_n) ratio (see Figure 2.8) and increase of the growth probability α_n with chain length (see Figure 2.17). Three different proposals for chain length dependent processes in the FTS were given by Kuipers et al. [103]:

1. n-dependent diffusion limitations [89, 93, 112, 113]

2. n-dependent solubility in the FT-wax [64, 92, 103, 114, 115]

3. n-dependent physisorption [64, 92, 101, 103]

Therefore, the interfacial effects of reactive olefins near the gas-wax and wax-catalyst surfaces are important. Figure 2.18 (obtained from Kuipers et al. [103]) gives a schematic representation of the olefin concentration profile on a catalyst with a wax

layer. The concentration of the olefins dissolved in the wax phase ($x = d$) can be related to the vapor-phase concentration. Steady state production of olefins results in a concentration gradient over the wax film, which depends on the production rate of olefins, film thickness (d) and the diffusivity of product with chain length n (D_n). At the wax-catalyst interface ($x = -\delta$) n-dependent physisorption will take place. The chain length dependencies of physisorption, solubility, and diffusivities will be discussed below. First, we will consider possible secondary reactions that can take place on FT catalysts.

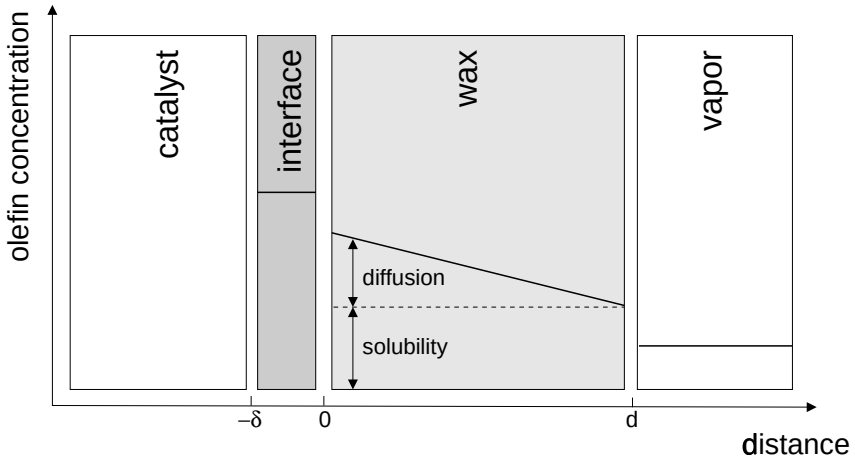

Figure 2.18 Schematic olefin concentration profile on a wax-coated catalyst (from Kuipers et al. [103]).

2.7.2.2 Secondary Reactions

In general, the extent of secondary reactions increases in the order: Fe, Ru, Co [93, 116, 117]. Because of the relatively low tendency of Fe for secondary reactions, high olefin yields can be obtained with alkali promoted iron catalysts. The extent of secondary reactions can also be observed from the dependency of the (O_n/P_n) ratio or olefin content on chain length, see Figure 2.8. On Fe-, Ru-, and Co-based catalysts an exponential decrease with chain length is observed [103]:

$$\frac{m_{O_n}}{m_{P_n}} \propto e^{-Cn} \tag{2.10}$$

Table 2.4 Carbon number dependencies on olefin to paraffin ratio ($n > 3$) according to $m_{O_n}/m_{P_n} \propto e^{-Cn}$.

Catalyst	C	T (K)	P (MPa)	H_2/CO	Conversion	Ref.
Uncoated cobalt foil	0.59	493	0.10	2		[103]
Wax-coated cobalt foil	0.24	493	0.10	2		[103]
Co/TiO_2	0.49	473	2.0	2.1	X_{CO} 9.5 %	[3]
Co/TiO_2	0.25	473	2.0	2.1	X_{CO} 72 %	[3]
Ru/TiO_2	0.38	476	0.56	2.1	X_{CO} 5 %	[3]
Co/TiO_2	0.19	476	0.56	2.1	X_{CO} 60 %	[3]
Fe/Cu/K	0.15	489	1.62	2		[32]

where m_{O_n} and m_{P_n} are the production rates or mole fractions of olefins and paraffins with carbon number n and C is a constant. See Table 2.4 for several literature values of C. The ratio of olefins to paraffins depends on catalyst type and structure, and reaction conditions. Iglesia et al. [3] observed a two-fold decrease of the exponential factor, C, for cobalt and ruthenium catalysts, when the residence time in a packed bed reactor decreased from 12 to 2 seconds corresponding to 9.5 % and 72 % CO conversion, respectively (see Table 2.4).

A direct indication of secondary reactions can be obtained from co-feeding of olefins (see Table 2.5 for a summary of references). In studies with carbon-labeled olefins, low concentrations can be used. Non-labeled co-fed olefins must have higher concentrations (5-10 mol %) to observe significant effects of possible secondary reactions. Different from co-fed olefins, an olefin produced on a growth site obtains physisorbed interactions with the catalyst surface, at least for some time. Therefore, reactivity of co-fed olefins may differ from the adsorbed olefin intermediate products. This makes interpretation of such experiments complicated and tricky.

In Table 2.5, the selectivity of secondary reactions: i) hydrogenation, ii) isomerization, iii) reinsertion, and iv) cracking or hydrogenolysis is calculated as the fraction of the co-fed olefin converted by a specific reaction relative to the total conversion of that olefin added.

Most olefin co-feeding studies were performed at atmospheric pressure. Under real FTS reaction conditions (high CO and H_2O pressures), secondary reactions can be inhibited. Almost all results of co-feeding of olefins show a significant amount of secondary hydrogenation [89, 102, 114, 116, 118–121]. Added olefins are hydrogenated to the corresponding paraffin.

Table 2.5 Summary of co-feeding studies olefins.

		Selectivity of co-fed olefins (%)			
Reference	Component	Hydr.	Reins.	Isom.	Cracking
Schulz et al. [116]	ethene	67	29	-	4
	propene	51	31	-	12
	1-hexadecene	79	6	-	14
Schulz et al. [116]	ethene	88	12	-	< 1
	propene	96	3	-	< 1
Schulz et al. [118]	1-octene	15	33	52	-
		20	30	50	-
		10	35	55	-
		5	35	60	-
Hanlon and Satterfield [119]	ethene	92	8	-	-
		94	6	-	-
	1-butene	31	67	2	-
Tau et al. [114]	ethene[3]	64-73	18 (C_{5+})	-	-
	1-pentene	-	-	-	-
	1-decene	43	-	57	-
Jordan and Bell [102][2]	ethene	95	4.2	-	-
		58	42	-	-
		50	50	-	-
		51	49	-	-
		38	62	-	-
Jordan and Bell [120][2]	propene	98	2.1	-	-
		92	8.1	-	-
		89	11	-	-
		90	10	-	-
		92	8.1	-	-
Jordan and Bell [121][2]	1-butene	62	4.2	34	-
		48	4.8	52	-
		38	5.2	57	-
		20	6.6	74	-
		21	6.6	72	-
Iglesia et al. [89]	ethene	50.5	49.5	-	-
		11.5	88.5	-	-
Iglesia et al. [89]	ethene	70.5	29.5	-	-
		22.0	78.0	-	-

Notation: Hydr.= Hydrogenation, Reins.= Reinsertion, Isom.= Isomerization

[1] First line gives general operating conditions. Following lines denotes the parameters changed

[2] Selectivity of reinsertion and hydrogenolysis are added in column Reins. The influence of CO pressure is presented only.

[3] Selectivity of co-fed ethene to 1-propanol is about 9-18 %.

Table 2.5 Continued from previous page; operating conditions and catalyst applied.

Reference	Catalyst, Reactor	Operating conditions[1]
[116]	$Co/ThO_2/K$, fixed bed	T = 185-190 ˚C, H_2/CO=2, P= 0.1 MPa
[116]	Iron, fixed bed	T = 220 ˚C, H_2/CO=2, P= 2.0 MPa
[118]	Cobalt, slurry	T = 180 ˚C, P_{H_2}=0.5 MPa, P_{CO}=0.5 MPa
		P_{CO}=1.0 MPa
		P_{CO}=1.5 MPa
		P_{CO}=2.0 MPa
[119]	Fe/K, slurry	T = 248 ˚C, P_{CO}=0.08 MPa, P_{H_2}=0.23 MPa
		P_{CO}=0.34 MPa, P_{H_2}= 0.33 MPa
		P_{CO}=0.071 MPa, P_{H_2}= 0.27 MPa
[114]	Iron, slurry	T=260 ˚C, P=0.70 MPa, H_2/CO=1.2
[102][2]	Ruthenium,	T=493 K, P_{H_2}=0.04 MPa, P_{CO}= 0.00 MPa
	micro reactor	P_{CO}= 0.02 MPa
		P_{CO}= 0.05 MPa
		P_{CO}= 0.10 MPa
		P_{CO}= 0.20 MPa
[120][2]	Ruthenium,	T=493 K, P_{H_2}= 0.03 MPa, P_{CO}=0.00 MPa
	micro reactor	P_{CO}= 0.01 MPa
		P_{CO}= 0.05 MPa
		P_{CO}= 0.10 MPa
		P_{CO}= 0.20 MPa
[121][2]	Ruthenium,	T=493 K, P_{H_2}= 0.04 MPa, P_{CO}=0.00 MPa
	micro reactor	P_{CO}= 0.02 MPa
		P_{CO}= 0.05 MPa
		P_{CO}= 0.12 MPa
		P_{CO}= 0.20 MPa
[89]	Ruthenium,fixed bed	T= 465 K, P= 2.07 MPa, H_2/CO=2
		15 mol% H_2O
[89]	Cobalt, fixed bed	T=465 K, P=2.07 MPa, H_2/CO=2
		15 mol% H_2O

Secondary hydrogenation is inhibited by CO [89, 102, 118–121] suggesting competitive adsorption of olefins and CO for the same catalytic sites. For example, Hanlon and Satterfield [119] observed a decrease of the added ethene conversion from 59 % to 9.2% when the CO pressure was increased from 0.08 MPa to 0.34 MPa on a potassium-promoted fused magnetite catalyst.

Schulz and Gökcebay [117] mentioned secondary hydrogenation as the most important process for the selectivity of the FT products on iron catalysts promoted with one of the transition metals Mn, Ti, Cr, Zr, or V. They concluded that secondary hydrogenation increases with carbon number due to increased adsorption strength. Ethene appeared very reactive for hydrogenation relative to propene and butene. Mechanistic conclusions from their results are that FT catalyst sites produce preferably olefins and to a smaller extent paraffins and that olefins can be adsorbed and hydrogenated on hydrogenation sites which are of another type than the Fischer-Tropsch growth sites. The authors stated that these hydrogenation sites can be inactivated in matrix catalysts, but no direct evidence on the nature of these sites was given.

No cracking or hydrogenolysis reactions of co-fed olefins (ethene, 1-butene, 1-hexene, 1-decene) was observed by Hanlon and Satterfield [119]. Also Dwyer and Somorjai [122] did not observe any cracking products from added ethene or propene. Schulz et al. [116] reported less than 1% cracking of added ethene or propene on an iron catalyst. However, cracking of added olefins was observed by Jordan and Bell [102, 120, 121] on a ruthenium catalyst at low total pressure. Cracking is promoted by high hydrogen pressures and high temperatures ($T > 300$ °C) and is strongly inhibited by CO pressure [13, 123] and H_2O pressures [113]. Therefore, we conclude that cracking is unimportant under normal FT synthesis conditions on Co and Fe catalysts [116, 124]. Under certain conditions, for example, high temperatures (hot spot) or a high degree of CO conversion (large catalyst pellets or low H_2/CO ratio), cracking of hydrocarbons may occur [89].

Insertion or readsorption of co-fed olefins was observed by many authors [89, 102, 114, 116, 118–121]. Insertion of olefins reverses the chain termination step to olefins and causes an increase of the chain growth probability and decrease of the olefin content of the products. Hanlon and Satterfield [119] observed an increased selectivity of C_{3+} hydrocarbons with addition of ethene on an Fe/K catalyst. Likewise, addition of 1-butene or 1-hexene resulted in a minor increase of the yield of high-molecular products, suggesting olefins to act as chain initiators. Addition of ethene and ethanol also resulted in a lower methane selectivity and increased olefin to paraffin ratio for C_3 and C_4 according to Hanlon and Satterfield [119]. Ethanol and ethene reduced the

hydrogenation of olefins on the catalyst. Addition of olefins and ethanol did not result in a change of the chain growth factor, α.

Iglesia et al. [89] showed the difference between co-fed ethene and *in situ* formed ethene on Ru and Co catalysts. Studies of the variation of bed residence time showed that 95% of the *in situ* formed ethene is consumed as chain initiator, while less than 5% appears as hydrogenated product. Co-feeding of ethene resulted in much higher selectivities towards ethane ($\approx$ 50%). They also found that the reactivity of added α-olefins in chain initiation reactions on Ru catalysts decreased in the order [93]:

$$\text{ethene} \gg \text{propene} \geq \text{1-butene} \approx C_{5+}\ \alpha\text{-olefins}. \tag{2.11}$$

Iglesia et al. [3] showed an increase of the olefin selectivity with increasing flow rate on a Co/TiO_2 catalyst, due to secondary reactions. The paraffin selectivity remained independent of the bed residence time for small paraffins, suggesting that hydrogenation is not the most important secondary reaction. The selectivity to higher molecular weight paraffins decreased with increasing flow rate due to accumulation and high surface concentration of smaller alkyl chains. The selectivity to methane increases, while the selectivity to C_{5+} products decreases with increasing space velocity (decreasing residence time) (see Figure 2.10). Therefore, they suggested that olefins are not consumed in secondary cracking or hydrogenation reactions. The same observations were reported by Komaya and Bell [101] for C_2 and C_4 products on a Ru/TiO_2 catalyst at 523 K. Iglesia et al. [3, 89], Madon et al. [32], and Komaya and Bell [101] concluded that readsorption of α-olefins and chain initiation is the most important secondary reaction for Ru, Co, and Fe resulting in deviations from the ASF distribution instead of hydrogenation or hydrogenolysis reactions.

Secondary hydrogenation is strongly inhibited by CO. Table 2.5 shows that the rates of isomerization and reinsertion are less inhibited by CO [89, 102, 113, 119, 120]. At high CO pressures, reinsertion of olefins becomes more important. Some data on the influence of H_2O on secondary reactions was reported by Iglesia et al. [89]. Addition of 15 mol% H_2O to synthesis gas (T= 465 K, H_2/CO=2, P= 2.07 MPa) on a ruthenium and cobalt catalyst resulted in reinsertion of ethene to be the most important secondary reaction (see Table 2.5). Also, Hall et al. [125] observed a strong decrease of secondary hydrogenation of added ethene, with addition of 1.6 % water vapor on a $Zr/Fe/Al_2O_3$ catalyst.

Co-fed α-olefins can also isomerize to internal olefins (cis- and trans-β-olefins). Isomerization of 1-octene on a cobalt catalyst is favored by high CO pressure, while secondary olefin hydrogenation is inhibited [118].

From this discussion, we conclude that secondary reactions of olefins on iron, cobalt, and ruthenium catalysts are responsible for the observed selectivities. The most important secondary reaction is readsorption of olefins resulting in initiation of chain growth processes. Secondary hydrogenation of olefins is observed for added olefins but seems to be a minor reaction for *in situ* formed olefins. Moreover, high CO and H_2O pressures inhibit hydrogenation and cracking reactions in comparison to olefin readsorption. Secondary hydrogenation may occur under certain conditions, depending on the catalytic system and the process conditions (high H_2 pressures).

2.7.2.3 Chain Length Dependency of the Secondary Reactions

Secondary reactions of olefins depend on the chain length, resulting in a decrease of the (O_n/P_n) ratio and increase of the growth probability α_n with chain length. The influence of three possible chain length dependent processes are discussed below.

Diffusivity

Both diffusion limitation of reactants to the catalytic sites, and of products from the sites may occur. Slow removal of reactive products (for example, α-olefins) due to a decrease of diffusion coefficients with increasing chain length can influence the FTS reaction rate and selectivity. Measurements of these coefficients at FT operating conditions are scarce. Erkey et al. [126] measured the molecular diffusion coefficients of three paraffins (n-octane, n-dodecane and n-hexadecane) in FT-wax with an average chain length of C_{28} (see Figure 2.19). Using the correlation proposed by Wilke-Chang [127] to predict the molecular diffusivity of hydrocarbons in a heavy paraffinic Fischer-Tropsch product (viscosity wax with M= 300 g/mol, at T= 504 K: μ= 0.6 x 10^{-3} N s m^{-2}) we found a chain length dependency of $D_n \propto n^{-0.5}$. The calculated values for the diffusivities of C_1 to C_{17} are also plotted in Figure 2.19.

Iglesia and co-workers studied the influence of chain length dependent diffusion coefficients on secondary reactions [3, 32, 89, 93, 112, 113, 128]. They reported an empirical equation describing a strong influence of chain length on diffusivity for olefins and paraffins $D_n \propto e^{-0.3n}$, which was not verified by experimental data. This carbon number dependency is a factor of three higher than determined by Erkey et al. [126] and apparently is wrong (see Figure 2.19).

Iglesia et al. [89] modeled diffusion-limited removal of olefins and diffusion limitation of CO on a cobalt and ruthenium catalyst in a packed bed reactor. No reactant depletion was observed at particle diameters smaller than 0.2 mm. However, selectivity changes due to product limitations are still present. They concluded that olefin

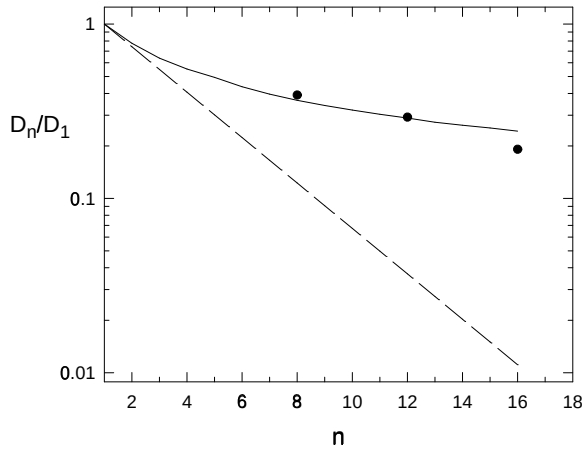

Figure 2.19 Diffusivities of n-paraffins in FT-wax; • experimental data at T= 504 K from Erkey et al. [126], — Wilke-Chang correlation at T= 540 K, - - - correlation Iglesia et al. [89].

readsorption and chain initiation is the most important secondary reaction. Their transport model includes the rate of diffusion-enhanced olefin readsorption and its effect on detailed product distributions. However, Iglesia et al. [89] were not able to explain the strong exponential decrease of the (O_n/P_n) ratio on their catalyst (C= 0.19-0.49 in eq 2.10) with diffusion effects only. Especially, when the more realistic lower dependency of the diffusion coefficients with chain length, as observed by Erkey et al. [126] (see Figure 2.19), is used their model underestimates the olefin to paraffin ratio.

Furthermore, Kuipers et al. [103] measured the (O_n/P_n) ratio for the FTS on a polycrystalline cobalt-foil (without diffusion limitations) and still obtained an exponential decrease of this ratio with chain length. So, we can conclude that the chain length dependency of the olefin to paraffin ratio can hardly be due to diffusion effects only, but that preferential physisorption and increase of the solubility with chain length influences the selectivity as well.

Solubility

Values of the vapor–liquid equilibria (VLE) of reactants and products in high-boiling solvents are necessary for an optimal design of gas-slurry processes and kinetic modeling. Experimental data of solubilities at high pressures are scarce in open literature.

Solubilities are often expressed in terms of Henry's constants of a solute in a solvent:

$$H_{1,2} = \lim_{x_1 \to 0} \frac{f_1}{x_1} \tag{2.12}$$

where f_1 is the fugacity of the solute and x_1 is its mole fraction in the liquid phase.

Breman et al. [129] studied 1533 VLE for 60 binary systems of the reactants: carbon monoxide, hydrogen and products: water, carbon dioxide, C_1-C_6 alcohols and C_2-C_6 paraffins in the solvents tetraethylene glycol, hexadecane, octacosane, 1-hexadecanol, and phenantrene. Experimental conditions were varied from 293 to 553 K and from 0.06 to 5.5 MPa. Measurements of the VLE of reactants and products in octacosane closely resemble FTS operating conditions.

Chappelow and Prausnitz [130] measured the solubilities of n-paraffinic gases C_1-C_4 in high-boiling hydrocarbon solvents at low-pressures in an equilibrium cell. A gas-chromatographic technique was used by Donohue et al. [131] to measure the solubilities of n-paraffins (C_5-C_9) in solvents. Figure 2.20 shows the logarithm of the Henry's constant as a function of the carbon number of the solute in eicosane (C_{20}). Henry's coefficients obtained from Donohue et al. [131] are interpolated to T= 325 K. At this temperature, the Henry's coefficients appear to decrease exponentially with carbon number, indicating an increase of the solubility with carbon number. VLE measured by Breman et al. [129] contain data for ethane, propane, pentane, and hexane in octacosane (C_{28}). Henry's constants were determined between T= 423 - 518 K. Figure 2.20 also shows these constants as a function of carbon number at three temperatures. As aspected, the solubility decreases with increase in temperature for all components. The available VLE data show that carbon number dependency decreases with increasing temperature (Figure 2.20).

A rough estimate of the ideal solubility can be found using Raoult's law [127] and vapor pressure data of hydrocarbons. Caldwell and van Vuuren [132] found that the vapor pressures of n-paraffins C_9 to C_{29} (T= 452-553 K) can be described with the following equation:

$$P_n = P_0 \beta^n \tag{2.13}$$

where P_n is the vapor pressure of a paraffin with a chain length n and P_0= 17.8382 MPa and $\beta = \exp[-427.218(1/T - 1.029807x10^{-3})]$. The vapor pressure (and solubility), calculated with eq 2.13, as function of temperature is also plotted in Figure 2.20. It can be seen that the exponential chain length dependency of the vapor pressure ($\exp\beta$) is in good agreement with the experimental VLE data [129] although these experimental values were obtained with short-chain hydrocarbons ($n < 6$).

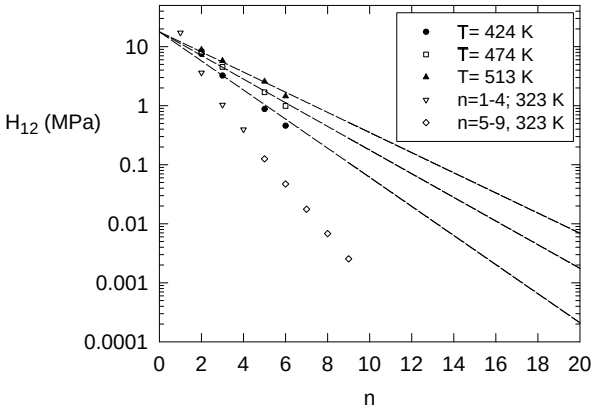

Figure 2.20 Henry's constants of n-paraffins in eicosane at T = 323K (Chappelow and Prausnitz [130] and Donohue et al. [131]) and in octacosane at T = 424, 474, and 513 K (Breman et al. [129]), dotted lines are calculated with the vapor pressure correlation for C_9-C_{29} (Caldwell and van Vuuren [132]).

Much controversy exists on the effect of the solubility on the reaction rate of secondary reactions. Schulz et al. [74], Tau et al. [114], Zimmerman et al. [115] and Kuipers et al. [103] stated that a greater solubility of larger hydrocarbons results in an increase of the residence time and higher readsorption rates. Madon and Iglesia [112] and more recently Iglesia [133] rejected the arguments of solubility stating that the presence of a liquid does not influence chemical potentials. They concluded that the presence of a liquid phase in absence of transport limitations, cannot increase the rate of secondary reactions. They accounted the deviations from the ASF distribution completely to diffusion-enhanced readsorption of α-olefins. However, as seen above, this is not convincing.

According to our opinion, indeed an "ideal" liquid does not influence the reaction rate. Here, "ideal" means an inert, non-adsorbing, non-polar liquid with all activity coefficients equal to unity whilst no mass transfer affects are apparent. This follows from transition-state theory, where the chemical potential (fugacity at standard state) of any component is the same in the gaseous, liquid, and adsorbed state.

However, in real cases the liquid may affect the reaction rate. Eckert [134] considered a bimolecular reaction between two gases on a solid catalyst in presence of a liquid-phase. A reaction, $A + B \rightarrow$ product, in a system with thermodynamic non-

idealities, can be described with the Brønsted-Bjerrum equation:

$$k = \frac{k_0 \gamma_A \gamma_B}{\gamma_I} \tag{2.14}$$

where k_0 is the rate constant in an ideal reference state. The presence of a liquid may alter the activity coefficients of the reactants on the surface, γ_A or γ_B, and of the activated complex γ_I. To evaluate the effect of a liquid, Eckert [134] used regular solutions theory for dilute, non-polar solutions

$$RT \ln \gamma_A = V_2(\delta_A - \delta_1)^2 \tag{2.15}$$

Here subscripts A and 1 refer to the solute A and solvent, respectively. δ is the solubility parameter. Substitution into eq 2.14 gives

$$\ln k = \ln k_0 + \frac{V_A}{RT}(\delta_1 - \delta_A)^2 + \frac{V_B}{RT}(\delta_1 - \delta_B)^2 - \frac{V_I}{RT}(\delta_1 - \delta_I)^2 \tag{2.16}$$

There are two possible assumptions to evaluate the non-ideality of the system. The first assumption is that all surface species are in equilibrium with the activities in the bulk, which is given in the foregoing equation. The other possibility is that the reactants on the surface are in equilibrium with the bulk, while the activated complex is not. Then the activity of the complex might be independent of the liquid and its activity coefficients are constant. If so, we have [134]:

$$\ln k = \ln\left(\frac{k_0}{\gamma_I}\right) + \frac{V_A}{RT}(\delta_1 - \delta_A)^2 + \frac{V_B}{RT}(\delta_1 - \delta_B)^2 \tag{2.17}$$

Eckert [134] evaluated hydrogenation experiments and concluded that the second assumption is valid for heterogeneous reactions. If so, the rate of reaction is proportional to the concentration of the activated complex instead of its thermodynamic activity. eq 2.17 shows that the reaction rate is enhanced, compared to the rate in the ideal liquid or gas phase, if the solvent is similar to the reactants (high solubility) and vice versa.

Moreover, comparison of the increase of the transport rates of olefins with varying carbon number in analogy with eq 2.1 [3] shows:

$$\gamma_n = \frac{D_{O_n}/H_{O_n}}{D_{O_{n-1}}/H_{O_{n-1}}} \approx \frac{H_{O_{n-1}}}{H_{O_n}} \tag{2.18}$$

since solubility effects overrule the weak chain-length dependency of the diffusivity.

This discussion has a great impact on the rate of readsorption of olefins during the FTS. The solubility increases exponentially with carbon number. Consequently, the rate of readsorption of long-chain olefins is enhanced in comparison to smaller olefins (according to eq 2.17), because actual concentrations are necessary instead of activities. Kuipers et al. [103] also stated that the olefin concentration at the catalyst interface has to be taken into account for the readsorption rate, which is not in equilibrium with the chemisorbed phase at the catalyst surface.

Physisorption

Physisorption of hydrocarbons may change the extent of secondary reactions. The physisorbed state is a transition state between the chemisorbed and the vapor phase and is governed by Van der Waals attraction and repulsion forces [15]. These forces depend on the structure of the adsorbates and the adsorbents. Here, we focus on the influence of carbon number on the adsorption of hydrocarbons on adsorbents. Measurements of gas-solid adsorption of hydrocarbons on several adsorbents are reported in literature [135–137]. The logarithm of the adsorption equilibrium constant increases linearly with carbon number. Komaya and Bell [101] used a chain-length dependent Henry constant at 523 K for the readsorption of olefins on a ruthenium catalyst under FT conditions: $H_n \propto e^{1.2n}$.

Keldsen et al. [138] measured the enthalpies of adsorption of linear paraffins with different chain length on a clay. The enthalpy of adsorption and the strength of the physisorbed bond appeared to increase with carbon number. We used a linear regression of their experimental enthalpies of adsorption as a function of carbon number, n:

$$-\Delta H_{ad} = 12.6 + 8.7n \quad \text{(kJ/mol)} \tag{2.19}$$

This relation suggests a simple group-additive quantity for linear paraffins, as also mentioned by Ruthven [139] (originally from Kiselev and Shcherbakova [140]) for a homologous series of paraffins on silica:

$$-\Delta H_{ad} = 12.5 + 4.0n \quad \text{(kJ/mol)} \tag{2.20}$$

Ruthven [139] also reviewed a group contribution method for estimating the heat of adsorption on 5 Å zeolites. The presence of double bonds appears to give rise to a higher dipole moment for the adsorbed species resulting in a higher increment of the heat of adsorption.

Xia and Landman [141] reported the results of molecular dynamic calculations of the preferential adsorption of n-hexadecane and n-hexane on a Au(001) surface.

Starting with an equimolar mixture of the components resulted in a layer at the interface with high concentration of long-chain molecules due to a better packing and intermolecular ordering at steady state.

Rofer-De Poorter [7] schematically described the FT catalyst surface as a very active layer at the metal surface containing C,O, H atoms, adsorbed CO and growing alkyl chains; further away from the surface are physisorbed CO, H_2, and desorbing products. Reaction intermediates are also present in the surface layer. From the above, we conclude that the adsorption equilibrium constants increase exponentially with chain length resulting in an increase of the contact time and an enrichment of long-chain hydrocarbons at the catalyst surface.

Komaya and Bell [101] and Pichler and Schulz [124] reported the effect of stronger physisorption for larger olefins to predict the increase of the chain growth probabilities with chain length. Komaya and Bell [101] developed a model where desorption of chemisorbed products proceeds through a physisorbed layer. Transient kinetic experiments with labeled carbon were performed in a packed bed reactor at 523 K. Equations for labeled carbon in the monomer pool, the pool of alkyl chains, and the pool of physisorbed hydrocarbons were optimized to experimental data. The fractional coverage of products in the physisorbed layer, θ_n, was calculated with the chain length dependent Henry constant. The authors stated that for olefins with $n > 8$, readsorption becomes more important than removal of physisorbed hydrocarbons from the reactor.

We conclude from this discussion that the solubility and physisorption are crucial for the reaction rates in the FTS. Secondary reactions of olefins can be influenced by the chain length dependent solubility in a liquid and by preferential physisorption.

2.7.3 Comprehensive Product Distribution Models

The distribution of paraffins was firstly described by Herrington [142]. His approach used individual chain termination probabilities for each chain size, β_n,

$$\beta_n = \frac{R_{t,n}}{R_{p,n}} = m_n / \sum_{i=n+1}^{\infty} m_i \tag{2.21}$$

The chain growth probability, α_n can easily be calculated from eq 2.21:

$$\alpha_n = 1/(1+\beta_n) = \sum_{i=n+1}^{\infty} m_i / \sum_{i=n}^{\infty} m_i \tag{2.22}$$

Iglesia et al. [93] used the same approach and expressed the total termination probability ($\beta_{t,n}$) as a combination of individual terminations:

$$\beta_{t,n} = \beta_{t,O} + \beta_{t,P} - \beta_{R,n} \tag{2.23}$$

where $\beta_{t,O}$ and $\beta_{t,P}$ is the termination probability to olefins and paraffins, respectively. We showed above that Iglesia et al. [93] stated incorrectly that the readsorption of olefins ($\beta_{R,n}$) is chain length dependent due to diffusion effects alone. The chain termination probability in eq 2.23 and the O/P ratio decrease with increasing carbon number until all olefins are consumed. The asymptotical value of $\beta_{t,n}$ or α_n corresponds to propagation and termination to paraffins alone. However, the increased readsorption rate is not completely due to diffusion effects, increased solubility and physisorption with increasing carbon number should be taken into account.

Kuipers et al. [103] modeled the experimental data of the olefin to paraffin ratio synthesized on wax-coated and uncoated cobalt foils at atmospheric pressures and a temperature of 493 K. Mass balances over the film layer were given to obtain the concentration of olefins in the physisorbed layer, wax phase and vapor phase. According to the authors, the concentration of the olefins dissolved in the wax phase ($x = d$, see Figure 2.18) can be related to the vapor-phase concentration by Raoult's law and is proportional to $(C^s_{n\ vap} V^m_{n\ wax})^{-1}$, where $C^s_{n\ vap}$ is the saturated vapor phase concentration and $V^m_{n\ wax}$ is the molar volume of hydrocarbons with carbon number n. They used the following exponential increase for the solubility, $1/C^s_{n\ vap} \propto e^{(0.55\pm0.10)n}$ at 493 K and a linear increase of $V^m_{n\ wax}$ with n. Above, we described experimental and calculated data on the solubility of hydrocarbons. At a temperature of 493 K, the correlation of Caldwell and van Vuuren [132] shows that the solubility is proportional to $e^{0.43n}$. Kuipers et al. [103] described the increase of physisorption strength of hydrocarbons at the catalyst interface with increasing chain length by $e^{n\Delta G_{1phys}/RT}$. On uncoated foils without transport limitations (diffusion), their model predicts that $m_{O_n}/m_{P_n} \propto n \exp[-(\Delta G_{1phys}/RT + 0.55)n]$. Kuipers et al. [103] measured a carbon number dependency of $C = 0.55$ according to eq 2.10 on an uncoated cobalt foil. It can easily be seen that the authors stated incorrectly that the preferential physisorption is $\propto e^{0.2n}$, because in that case the exponent in eq 2.10 would be $C = 0.75$. This dependency is not the same as their experimental determined value of $C = 0.55$.

For small olefins and a wax-layer on the cobalt foil a much weaker chain length dependency was observed by Kuipers et al. [103] (see Table 2.4). Their model predicts the following chain length dependency on the O_n/P_n ratio when diffusion limitations

($D_n \propto n^{-0.6}$) are dominant:

$$O_n/P_n \propto e^{-n\Delta G_{1\ phys}/RT} D_n \propto e^{(-0.2\pm0.1)n} n^{-0.6} \tag{2.24}$$

In a more recent article, Kuipers et al. [92] concluded that the main secondary reaction on the same cobalt foil is secondary hydrogenation of primary α-olefins. With 50 nm Co particles on a SiO_2 wafer, Kuipers et al. [92] reported reinsertion of α-olefins as the most important secondary reaction.

We can conclude that any comprehensive product distribution model for the selectivity to olefins and paraffins should incorporate readsorption of olefins and the effect of physisorption and solubility on the actual olefin concentration at the catalyst surface. These models have to predict the selectivity to olefins and paraffins on porous FT catalysts at industrial conditions.

2.8 Kinetics

2.8.1 Introduction

The major problem in describing the FT reaction kinetics is the complexity of its reaction mechanism and the large number of species involved. As discussed above, the mechanistic proposals for the FTS used a variety of surface species and different elementary reaction steps, resulting in empirical power law expressions for the kinetics [8, 143]. However, also Langmuir-Hinshelwood-Hougen-Watson (LHHW) and Eley-Rideal type of rate equations have been applied, based on a reaction mechanism for the hydrocarbon forming reactions [22, 75, 144]. In most cases the rate determining step was assumed to be the formation of the monomer [22, 73, 145, 146]. These rate expressions for the consumption of synthesis gas mainly differ in the nature of the monomer and of the adsorption of CO, H_2 and products (H_2O and CO_2) on the catalyst surface.

Kellner and Bell [147] and Takoudis [148] modeled the production rates of hydrocarbons without assumptions on a rate determining step. However, several assumptions were introduced to solve the resulting set of equations. Lox and Froment [75] and Hovi et al. [76] examined whether the incorporation of the monomer or the termination reaction to hydrocarbons are rate limiting. Ideally, the development of kinetic rate expressions should be based on each possible rate determining process in a well-defined mechanistic scheme in the hydrocarbon-forming reactions.

Kinetic studies of the consumption of synthesis gas on iron and cobalt catalysts will be discussed in more detail, as well as kinetic studies of the WGS on iron cata-

lysts. Finally, kinetic models which describe the rate of formation of products will be reviewed.

2.8.2 Overall Conversion of Synthesis Gas

Kinetic equations can be based on the overall synthesis gas consumption (-R_{H_2+CO}= $-R_{CO} - R_{H_2}$), which is independent of the WGS equilibrium, or based on CO consumption to hydrocarbon products ($R_{FT} = -R_{CO} - R_{WGS}$). The rate of synthesis gas consumption only differs from the FT reaction rate by reaction stoichiometry, $-R_{H_2+CO} = (2 + m/2n)R_{FT}$. Reaction rate equations use to be expressed in either liquid phase concentrations or, preferably, in gas phase partial pressures. Since Henry's constants are temperature dependent, activation energies will also be influenced by the use of either liquid or gas concentration terms [56, 145].

The kinetic rate equations presented for the synthesis gas consumption [24, 56, 72, 149] do not present a uniform picture. Table 2.7 gives an overview. A few, mainly older, kinetic studies are performed in fixed-bed reactors at high synthesis gas conversions. Integral kinetic studies of the FTS in plug flow reactors (PFR) are not easily interpreted because the partial pressure of CO and H_2 as well as the composition of the catalyst vary along the axis of the reactor [22]. Extra complications occur due to possible heat and mass transfer effects, secondary reactions, and product inhibition. In general, catalyst composition as well as reaction conditions determine the numerical values of the intrinsic rate parameters. Moreover, the rate equations are not identical, thus k can be composed of different combinations of kinetic and adsorption constants. There is experimental evidence that the Fischer-Tropsch activity of Fe and Co depends on the preparation method, metal loading of the catalyst, and catalyst support [103, 150–154].

2.8.2.1 Iron Based Catalysts

Reviews of kinetic equations for iron catalysts are given by Huff and Satterfield [72] and Zimmerman and Bukur [56]. Kinetic studies of the FTS on iron catalysts are tabulated in Table 2.7.

In general for iron catalysts, the FT reaction rate increases with H_2 partial pressure and decreases with partial pressure of water. Satterfield et al. [164] observed a reversible decrease of the catalyst activity by addition of 12 and 27 mol% water to the feed gas. However, after addition of 42 mol% water the catalyst did not regain its initial activity.

Table 2.6 Reaction rate equations overall synthesis gas consumption rate, proposed in the studies mentioned in Table 2.7.

	Kinetic expression	References
(a)	$k P_{H_2}$	[24, 56, 155]
(b)	$k P_{H_2}^{a} P_{CO}^{b}$	[143]
(c)	$\frac{k P_{H_2} P_{CO}}{P_{CO} + a P_{H_2O}}$	[24, 56, 156–158]
(d)	$\frac{k P_{H_2}^{2} P_{CO}}{P_{CO} P_{H_2} + a P_{H_2O}}$	[72, 158–160]
(e)	$\frac{k P_{H_2}^{2} P_{CO}}{1 + a P_{CO} P_{H_2}^{2}}$	[24]
(f)	$\frac{k P_{H_2} P_{CO}}{P_{CO} + a P_{CO_2}}$	[56, 145, 159, 161]
(g)	$\frac{k P_{H_2} P_{CO}}{P_{CO} + a P_{H_2O} + b P_{CO_2}}$	[56, 145, 161]
(h)	$\frac{k P_{CO}^{1/2} P_{H_2}^{1/2}}{\left(1 + a P_{CO}^{1/2} + b P_{H_2}^{1/2}\right)^{2}}$	[73]
(i)	$\frac{k P_{CO} P_{H_2}^{1/2}}{\left(1 + a P_{CO} + b P_{H_2}^{1/2}\right)^{2}}$	[22]
(j)	$\frac{k P_{CO} P_{H_2}}{(1 + b P_{CO})^{2}}$	[144, 162, 163]

Table 2.7 Kinetic studies for the FTS on cobalt and iron catalysts.

Catalyst	Reactor	Operating conditions			Kinetic expression	E_A (k)	$-\Delta$ H$_{ad}$ (a)	Ref.
		T, ˚C	P, MPa	H$_2$/CO$_{feed}$		(kJ/mol)	(kJ/mol)	
Fused Fe/K	Fixed bed	225-265	1.0-1.8	1.2-7.2	(a)	71	-	[155]
Prec. Fe/K/Cu	Slurry	235-265	1.5-3.0	0.6-1.0	(a)	86	-	[56][1]
Prec. Fe/K/Cu	Slurry	250	1.5-3.0	0.6-1.0	(c)	-	-	[56]
Iron	fixed bed	?	?	?	(c)	-	-	[24]
Fused Fe/K	Gradientless, fixed bed	250-315	2.0	2.0	(c)	85	8.8	[157]
Fused iron	slurry	232-263	0.4-1.5	0.5-1.8	(d)	83	100	[72]
Prec. iron	slurry	220-260	1.0	0.5-0.6	(f)	103	0	[161][2]
Prec. iron	slurry	220-280	0.5-1.2	0.5-3.5	(c)	89	-	[145][2]
Fused iron	slurry	210-270	0.5-5.5	0.5-3.5	(f)	81	-	[145][2]
Co/Kieselguhr	Berty	190	0.2-1.5	0.5-8.3	(h,i)	-	-	[22, 73][3]
Co/MgO/SiO$_2$	slurry	220-240	1.5-3.5	1.5-3.5	(j)	-	-	[163]
Co/Zr/SiO$_2$	slurry	220-280	2.1	0.5-2.0	(d)	97	-	[160]
Prec. Fe/Cu/K	Gradientless	230-264	1.0-2.6	1.1-2.4	(d)	56	-62	[158]
Prec. Fe/Cu/K	Gradientless	230-264	1.0-2.6	1.1-2.4	(c)	56	-60	[158]
Prec. iron	slurry	220-260	-	0.5-0.8	(f)	105	0	[159][2]
Prec. iron	slurry	220-260	-	0.8-2.0	(c)	80	55	[159][2]
Prec. iron	Fixed bed	250-350	0.6-2.1	3.0-6.0	-	-	-	[75][4]

[1]No temperature dependence of optimal rate equations (c) (Fe/Cu/K) and (g) (100 Fe/0.3 Cu/0.2 K) is given

[2]Rate equations expressed in liquid concentrations

[3]Only measurements at 190 ˚C are reported. Conversions and space velocities are not mentioned by Sarup and Wojciechowski [73]

[4]Kinetic expressions not mentioned in Table 2.6

The mechanistic kinetic rate expressions for iron catalysts are all based on the formation of the monomer species as the rate determining step in the consumption of synthesis gas. Several theories for the formation of the monomer species are postulated in literature: i) **Carbide mechanism**: here CO dissociates on the surface and the adsorbed carbon hydrogenates to a methylene species [18]. ii) **Combined enol/carbide mechanism**: here a methylene species is formed by hydrogenation of the hydroxylated enolic CO-H_2 complex [11]. Both mechanisms were discussed above (see Chapter 2.5). Huff and Satterfield [72] derived and reviewed kinetic equations 2.25 and 2.29 based on the formation of the monomer, methylene. The assumptions for the rate equations were: 1) The rate determining step is the reaction of dihydrogen and a carbon intermediate. 2) Carbon monoxide and water are strongly adsorbed on the catalyst surface. 3) Hydrogen is assumed to react molecularly via the gaseous phase or via the associated adsorbed state [18, 155].

Anderson [24] proposed a rate equation which included water inhibition:

$$R_{FT} = \frac{k P_{CO} P_{H_2}}{P_{CO} + a P_{H_2O}} \tag{2.25}$$

Dry [156] and Huff and Satterfield [72] derived the same equation from the combined enol/carbide mechanism, assuming strong adsorption of CO and water relative to H_2 and CO_2. Atwood and Bennett [157] used eq 2.25 to describe the kinetics on a fused nitrided iron catalyst. The activation energy was determined as E_A= 85 kJ/mol for the kinetic constant k and an adsorption enthalpy of -ΔH_{ad}= 8.8 kJ/mol for the adsorption parameter a:

$$k = k_\infty \exp(-E_A/RT) \tag{2.26}$$

$$a = a_\infty \exp(-\Delta H_{ad}/RT) \tag{2.27}$$

Shen et al. [158] modeled their data with the same rate expression and reported an activation energy of 56 kJ/mol for k and an adsorption enthalpy of -ΔH_{ad}= - 60 kJ/mol for a on a precipitated commercial Fe/Cu/K catalyst. The observed activation energy for the kinetic constant is low in comparison to most activation energies for Fischer-Tropsch reaction rates which are between 70 and 105 kJ/mol [56, 72]. Boudart [165] gives a list of the physical meaning of the most common rate parameters. For the adsorption enthalpy: -$\Delta H_{ad} > 0$. The adsorption constant is a combination of the adsorption constant of carbon monoxide and for water. Consequently, the heat of adsorption for water is 60 kJ/mol larger than for carbon monoxide adsorption.

At conversions of H_2 + CO conversion lower than 60% and in the case of a high shift activity of the catalyst, eq 2.25 can be simplified to a first order dependency in H_2, due to low partial pressures of water [24, 156]:

$$R_{FT} = k P_{H_2} \tag{2.28}$$

Dry et al. [155] measured FT kinetics on a fused, promoted iron catalyst in a differential fixed bed reactor, and found the behavior described by eq 2.28 with an activation energy of 71 kJ/mol.

Huff and Satterfield [72] observed a linear decrease in the adsorption parameter a in eq 2.25 with hydrogen pressure on a fused iron catalyst and incorporated this by modifying eq 2.25 to:

$$R_{FT} = \frac{k P_{CO} P_{H_2}^2}{P_{CO} P_{H_2} + a' P_{H_2O}} \tag{2.29}$$

note that a' in eq 2.29 equals a/P_{H_2} in eq 2.25. Equation 2.29 can be obtained from the carbide theory as well as from the enol/carbide theory which have identical mathematical descriptions (see Huff and Satterfield [72] for the derivation of these rate equations). Deckwer et al. [159] used eq 2.29 to describe the kinetic results for H_2/CO feed ratios between 0.8-2.0 on a potassium-promoted iron catalyst in the slurry phase. However, at low H_2 to CO feed ratios this equation was not able to describe the results due to high water gas shift activity. Shen et al. [158] used eq 2.29 to model their data and reported an activation energy of 56 kJ/mol for k and an adsorption enthalpy of $-\Delta H_{ad}$=-62 kJ/mol for a on a precipitated commercial Fe/Cu/K catalyst. The authors did not discriminate between the models in eq 2.25 and 2.29 on the basis of goodness of fit.

The water gas shift can increase or decrease the Fischer-Tropsch synthesis reaction rate by altering the concentrations of the reactants and products. Generally, CO_2 inhibition is not as strong as water inhibition due to the large difference in adsorption coefficients [10, 56]. However, iron catalysts with a high activity of the water gas shift reaction convert a significant amount of water into CO_2. Ledakowicz et al. [161], Nettelhoff et al. [145] and Deckwer et al. [159] reported the following equation including CO_2 inhibition:

$$R_{FT} = \frac{k P_{CO} P_{H_2}}{P_{CO} + a P_{CO_2}} \tag{2.30}$$

Ledakowicz et al. [161] used a precipitated iron catalyst (100 Fe/1.3 K) with high WGS activity and Nettelhoff et al. [145] a commercial fused iron ammonia synthesis

catalyst (BASF S6-10). Ledakowicz et al. [161] proposed a generalized rate expression for iron catalysts with high and low WGS activity:

$$R_{FT} = \frac{k P_{CO} P_{H_2}}{P_{CO} + a P_{H_2O} + b P_{CO_2}} \tag{2.31}$$

However, co-feeding of CO_2 to the feed gas showed that the CO_2 addition does not alter the reaction rate of the synthesis gas consumption significantly [166, 167]. Yates and Satterfield [167] suggested that the inhibition attributed to CO_2 [145, 159, 161] on catalysts with a high shift activity is caused by H_2O, since the reaction is at or close to equilibrium on these catalysts:

$$P_{CO_2} = K_P \frac{P_{CO} P_{H_2O}}{P_{H_2}} \tag{2.32}$$

where K_P is the equilibrium constant for the water gas shift reaction.

Figure 2.21 shows the response of the reported rate equations to a change in partial pressure of H_2, CO, H_2O, and CO_2, respectively. All equations observe an increase with partial pressure of H_2 and CO, while the other components inhibit the reaction rate. The large variation in the predictions is due to different inhibition effects and functional forms of the rate equations. The water gas shift activity of iron catalysts is of great importance for the inhibiting effects of water and possibly CO_2. Therefore, kinetic expressions can only be compared accurately if the optimal kinetic expression for the WGS is included. Only a CSTR model for the reactants as well as the products CO_2 and H_2O is adequate to compare different expressions. Kinetic expressions and mass balances have to be solved simultaneously. Figure 2.22 compares the results of FT and WGS kinetic expressions of three studies with iron catalysts [56, 158]. The overall conversion of synthesis gas is calculated as a function of the space velocity at 1.5 MPa, 523 K, H_2/CO feed ratio=1 in a CSTR. The kinetic equations applied are also shown in Figure 2.22. The kinetic study of Shen et al. [158] was performed in a gas-solid Berty reactor in contrast to the study with a slurry reactor used by Bukur et al. [91].

All proposed rate expressions were developed with the assumption that the rate determining step is the reaction of undissociated hydrogen with a carbon intermediate. The rate equations are valid only for the specific catalysts with WGS activity and for the process conditions used to develop the expressions. Therefore, we conclude that the development of FT kinetic equations still requires additional research. Detailed LHHW rate expressions tested both in gas-slurry and gas-solid reactors are needed for an accurate description of the consumption rates of the reactants during the Fischer-Tropsch synthesis on iron catalysts.

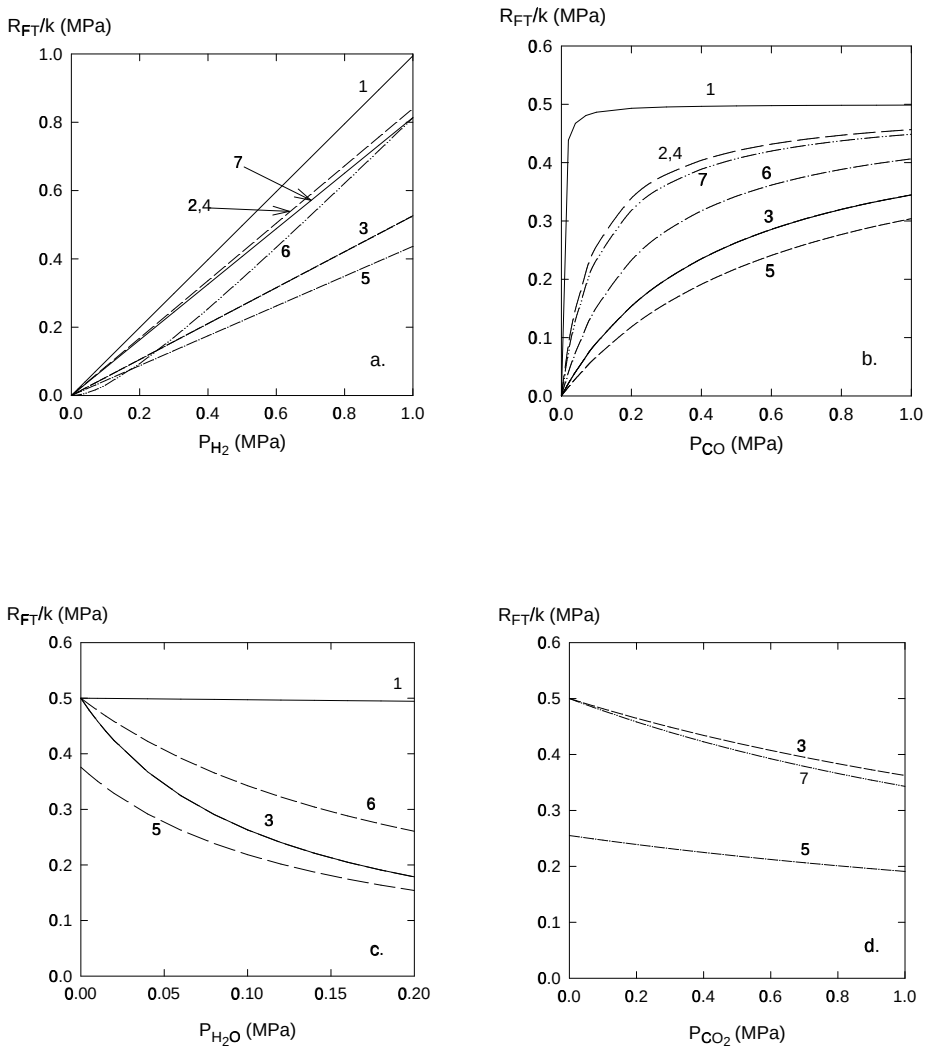

Figure 2.21 Relative reaction rates of synthesis gas consumption on iron catalysts. Kinetics expressions refer to Table 2.6. a) Influence of P_{H_2}: P_{CO}= 0.5 MPa, P_{CO_2}= 0.5 MPa, P_{H_2O}= 0.1 MPa. b) Influence of P_{CO}: P_{H_2}= 0.5 MPa, P_{CO_2}= 0.5 MPa, P_{H_2O}= 0.1 MPa. c) Influence of P_{H_2O}: P_{H_2}= 0.5 MPa, P_{CO}=0.5 MPa, P_{CO_2}= 0.5 MPa. d) Influence of P_{CO_2}: P_{H_2}= 0.5 MPa, P_{CO}=0.5 MPa, P_{H_2O}= 0.1 MPa. 1) Atwood and Bennett [157], 250 ˚C, a= 0.028, eq c 2) Nettelhoff et al. [145], 270 ˚C, a= 4.51, eq c (prec. Fe) 3) Nettelhoff et al. [145], 240 ˚C, b= 0.19, eq f (fused Fe) 4) Zimmerman and Bukur [56], 250 ˚C, a= 4.5, eq c (commercial Fe) 5) Zimmerman and Bukur [56], 250 ˚C, a= 4.8, b=0.33 eq g (prec. Fe) 6) Huff and Satterfield [72], 248 ˚C, a= 1.15 MPa, eq d (prec. Fe) 7) Ledakowicz et al. [161], 250 ˚C, b= 0.229, eq f (prec. Fe).

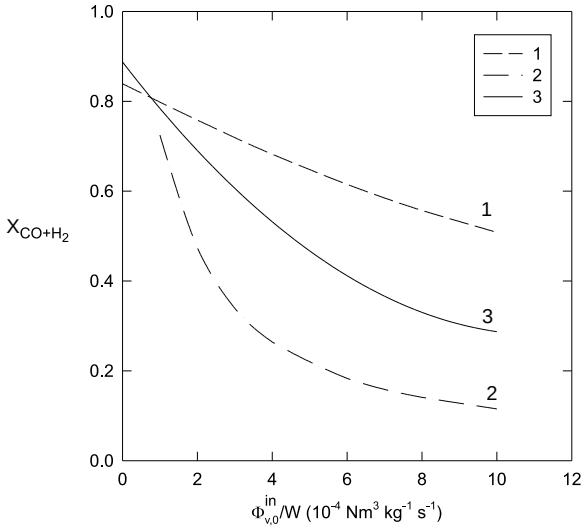

Figure 2.22 Activity comparison at different space velocities on iron catalysts at 1.5 MPa, 523 K, H_2/CO feed ratio= 1. 1) 100 Fe/0.3 Cu/0.2 K catalyst; R_{FT} eq g (Table 2.6) k=0.0222 mol kg_{cat}^{-1} s^{-1} MPa^{-1}, a= 4.8, b=0.33; R_{WGS} eq 2.37 k_w= 0.0133 mol kg_{cat}^{-1} s^{-1} MPa^{-1} (Zimmerman and Bukur [56]) 2) Fe/Cu/K commercial catalyst; R_{FT} eq c (Table 2.6) k= 0.00753 mol kg_{cat}^{-1} s^{-1} MPa^{-1} a= 0.472 ; R_{WGS} eq 2.39: k_w= 0.0987 mol kg_{cat}^{-1} s^{-1}, a= 0.692 MPa (Shen et al. [158]) 3) Fe/Cu/K commercial catalyst; R_{FT} eq c (Table 2.6) k= 0.0106 mol kg_{cat}^{-1} s^{-1} MPa^{-1} a= 4.5; R_{WGS} eq 2.39 k_w= 0.0122 mol kg_{cat}^{-1} s^{-1}, a= 0 MPa (Zimmerman and Bukur [56]).

2.8.2.2 Cobalt Based Catalysts

Only a few kinetic studies on cobalt based catalysts are available, see Table 2.7. Remarkably, nearly all kinetic expressions developed for cobalt based catalysts have a different form than for iron based catalysts. Generally, these kinetic equations are based on a rate determining step which involves a dual-site surface reaction, resulting in a quadratic denominator in the rate expression. Furthermore, inhibition terms of H_2O on cobalt catalysts are not reported in literature. Because the WGS reaction hardly plays a role on cobalt, no CO_2 is formed.

Wojciechowski [22] and Sarup and Wojciechowski [73] developed six different rate equations for the formation of the monomer (CH_2), based on both the carbide mechanism and the enol/carbide mechanism. The reaction rates were measured in a

Berty internally recycled reactor at 190 ˚C for P_{H_2} ranging from 0.07 to 0.68 MPa and P_{CO} between 0.003 and 0.93 MPa. All six rate expressions can be generalized as:

$$-R_{CO} = \frac{k P_{CO}^{a} P_{H_2}^{b}}{\left(1 + \sum_i K_i P_{CO}^{c_i} P_{H_2}^{d_i}\right)^2} \tag{2.33}$$

where k is a kinetic rate constant, a and b are the reaction orders of the rate determining step, K_i is the adsorption constant for the ith adsorption term, and c_i and d_i represent the dependency of surface coverage on the reactant pressure of the ith adsorption term. All six different models involve a bimolecular rate determining surface reaction step between a dissociated hydrogen species and a carbon intermediate. Testing of the kinetic models on their experimental data reduced the six to two equations:

$$-R_{CO} = \frac{k P_{CO}^{1/2} P_{H_2}^{1/2}}{\left(1 + K_1 P_{CO}^{1/2} + K_2 P_{H_2}^{1/2}\right)^2} \tag{2.34}$$

$$-R_{CO} = \frac{k P_{CO} P_{H_2}^{1/2}}{\left(1 + K_1 P_{CO} + K_2 P_{H_2}^{1/2}\right)^2} \tag{2.35}$$

In eq 2.34, the first hydrogenation of an adsorbed carbon atom and the first hydrogenation of an adsorbed oxygen atom are slower than the other reaction steps. The assumed rate determining step of eq 2.35 is the hydrogenation of adsorbed CO to form adsorbed formyl. However, after optimization of the parameters of eqs 2.34 and 2.35, the relative variance of experimental and calculated reaction rates was over 40 %, indicating a large lack of fit.

Yates and Satterfield [163] measured the kinetics of a cobalt catalyst in a slurry reactor. A Langmuir-Hinshelwood equation which also involves a bimolecular surface reaction, can accurately describe their results:

$$-R_{CO} = \frac{k P_{CO} P_{H_2}}{(1 + K_1 P_{CO})^2} \tag{2.36}$$

This equation was previously derived by Sarup and Wojciechowski [73] assuming hydrogenation of adsorbed formyl to form carbon and water to be rate determining. However, the number of inhibition terms was larger. Eq 2.36 fitted their data also best, but was rejected because one of the adsorption constants was negative. Yates and Satterfield [163] were able to fit the data of Sarup and Wojciechowski [73] well with the linearized form of the kinetic expression in eq 2.36.

The FT kinetics on a cobalt carbonyl catalyst in slurry-phase was measured by Whiters et al. [160]. They correlated the rate of CO and H_2 consumption to several kinetic equations used for the kinetics on iron catalysts (eqs 2.25 and 2.29). The best fit was obtained for eq 2.29 with an activation energy of 97 kJ/mol for the rate constant.

Recently, Ribeiro et al. [150] reviewed kinetic studies over cobalt FT catalysts in order to explain the differences in turnover rates. The available kinetic data were corrected to 473 K. Furthermore, the effects of partial pressure were corrected to a total pressure of 10 atm and H_2/CO= 2 with the use of a simple power law equation: $-R_{CO} = kP_{H_2}^{0.7}P_{CO}^{-0.2}$ which provided the best fit. The corrected turnover rates vary by a factor of 20, according to the authors due to the effect of a wide range of CO conversion and water concentration.

In comparison to iron catalyst is the kinetic research on cobalt catalysts more comprehensive. In the first place is the situation on cobalt catalysts easier due to the absence of the water gas shift reaction and less different catalytic sites. Secondly, Wojciechowski and co-workers [22, 73, 100, 168] described detailed LHHW equations based on a reliable mechanistic scheme for the CO consumption on cobalt catalysts. This approach is a good example of modeling complex reaction systems like the Fischer-Tropsch synthesis.

2.8.3 Water Gas Shift Kinetics

Cobalt catalysts are not active towards the WGS reaction in contrast to iron-based Fischer-Tropsch catalysts [54]. The water gas shift can increase or decrease the Fischer-Tropsch synthesis rate. Since these reactions share the same components, adsorption and desorption reactions as well as dissociation of H_2, H_2O, and CO_2 and reactions of formate species must be shared [169]. The individual WGS kinetics is studied extensively [54, 58, 81, 86], sometimes in combination with the methanation reaction [85] or methanol synthesis [82, 87]. Only a few studies reported the WGS kinetics of iron catalysts under FTS conditions. Table 2.8 gives an overview.

Based on unpublished results, Dry [156] reported the first (empirical) kinetic expression for the WGS reaction under FTS conditions which is independent of the water concentration:

$$R_{WGS} = k_w P_{CO} \tag{2.37}$$

The same equation was used by Feimer et al. [170] on a precipitated Fe/Cu/K catalyst, with an activation energy of 124 kJ/mol.

Table 2.8 Summary of kinetic studies of the WGS reaction (see also Table 2.7).

Kinetic expression	E_A (k_w) (kJ mol^{-1})	Reference
$R_{WGS} = k_w \left(P_{H_2O} P_{CO} - P_{CO_2} P_{H_2} / K_P\right)$		[56]
$R_{WGS} = k_w P_{CO}$	124[1]	[56, 156, 170]
$R_{WGS} = \dfrac{k_w \left(P_{H_2O} P_{CO} - P_{CO_2} P_{H_2}^{1/2} / K_P\right)}{\left(1 + a P_{H_2O} / P_{H_2}^{1/2}\right)^2}$	27.7	[75]
$R_{WGS} = \dfrac{k_w \left(P_{H_2O} P_{CO} - P_{CO_2} P_{H_2} / K_P\right)}{P_{CO} P_{H_2} + a P_{H_2O}}$	88[2]	[56, 158]
$R_{WGS} = \dfrac{k_w \left(P_{H_2O} P_{CO} - P_{CO_2} P_{H_2} / K_P\right)}{P_{CO} + a P_{H_2O} + b P_{CO_2}}$	125[2]	[56, 158]

[1] Activation energy Feimer et al. [170]

[2] Activation energy Shen et al. [158]

Since the WGS reaction is an equilibrium reaction at or close to equilibrium under Fischer-Tropsch reaction conditions the reverse reaction has to be taken into account. For the temperature dependency of the equilibrium constant of the WGS reaction, K_P, the following relation can be used [171]:

$$\log K_P = \log \left(\frac{P_{CO_2} P_{H_2}}{P_{H_2O} P_{CO}} \right)_{eq} = \left(\frac{2073}{T} - 2.029 \right) \tag{2.38}$$

Zimmerman and Bukur [56] measured the kinetics of the WGS reaction at 250 ˚C both on a home-made iron catalyst (100 Fe/0.3 Cu/0.2 K) and a commercial precipitated iron catalyst (Ruhrchemie LP 33/81). The experimental conditions are mentioned in Table 2.7. The 100 Fe/0.3 Cu/0.2 K catalyst obtained a higher WGS activity in comparison to the commercial catalyst, resulting in a higher extent of equilibrium and higher rate constants. The authors tested several kinetic models to their experimental WGS rates. Some of their kinetic equations contain the same functional form of the denominator as used in their kinetic equations of the FTS:

$$R_{WGS} = \frac{k_w \left(P_{H_2O} P_{CO} - P_{CO_2} P_{H_2} / K_P\right)}{P_{CO} P_{H_2} + a P_{H_2O}} \tag{2.39}$$

They also derived a kinetic expression with the denominator from the FT rate expres-

sion of Huff and Satterfield [72]:

$$R_{WGS} = \frac{k_w \left(P_{H_2O} P_{CO} - P_{CO_2} P_{H_2} / K_P\right)}{P_{CO} + a P_{H_2O} + b P_{CO_2}} \tag{2.40}$$

This implies that the reaction takes place on the same catalytic sites as the FT. No temperature dependency is given. The estimates of the adsorption constants were significantly different in comparison to the constants for the FT synthesis. If these reactions take place on the same catalytic sites, the adsorption constant may not differ. However, the authors stated that they were not able to derive reliable kinetic equations for the WGS kinetics under FT conditions and their results are largely empirical. For both catalysts applied, the adsorption constant b for CO_2 in eq 2.40 was not significantly different from zero. The modeling of the WGS kinetics for the 100 Fe/0.3 Cu/0.2 K catalyst was equally good with eq 2.39 and 2.40 and slightly better with the simple expression of eq 2.37. The reaction rate of the WGS for the commercial catalyst was best described with eq 2.39 with the adsorption coefficient a of H_2O equal to zero.

Shen et al. [158] measured the WGS kinetics on the same commercial catalyst in a gas-solid Berty reactor. See Table 2.7 for the experimental conditions.They fitted their data with the same equations and found activation energies for k_w in eq 2.39 and 2.40 of 88 kJ/mol and 125 kJ/mol, respectively. The adsorption constants appearing in the denominator were chosen equally to those in the FT kinetic equations, indicating that the authors also assumed that the two reactions proceed on the same catalytic sites.

Lox and Froment [75] also studied the FTS and WGS kinetics on the commercial precipitated iron catalyst (Ruhrchemie LP33/81). Discrimination between rival LHHW kinetic models resulted in the following optimal equation:

$$R_{WGS} = \frac{k_w \left(P_{H_2O} P_{CO} - P_{CO_2} P_{H_2}^{1/2} / K_P\right)}{\left(1 + a P_{H_2O} / P_{H_2}^{1/2}\right)^2} \tag{2.41}$$

In agreement with the statement of Rethwisch and Dumesic [58], the slowest step is the reaction between adsorbed CO and adsorbed hydroxyl species, resulting from the dissociation of water. They assumed the WGS reaction to proceed on a different catalytic site than the FTS. As discussed above, it is generally assumed for supported iron catalysts that magnetite is the most active phase for the WGS while the FT reactions proceed on iron carbides. The reported activation energy of 27.7 kJ/mol is relatively low in comparison to other kinetic studies, but consists of the contribution of adsorption enthalpies of reactants and products and a real activation energy. The

adsorption enthalpy of a was not significantly different from zero. It should be noted that these results were obtained in a packed bed reactor at high conversions, relatively high temperatures of 523-623 K, and high H_2/CO feed ratios between 3.0-6.0.

We conclude that the WGS kinetics under FT conditions still requires additional research. Lox and Froment [75] derived detailed LHHW rate expressions which should be tested on other studies with iron catalysts at common FT conditions both in slurry and gas-solid recycle reactors. Furthermore, knowledge about the active sites of the FTS and the WGS should provide more information for the kinetic modeling of this reaction network.

2.8.4 Hydrocarbon Production Rate

The hydrocarbon production rates on a potassium-promoted Fe_2O_3 catalyst have been correlated empirically by Dictor and Bell [51] as power law kinetics:

$$R_{C_n} = k_n P_{H_2}^a P_{CO}^b \tag{2.42}$$

The rate of formation of the hydrocarbons appeared to increase with P_{H_2}. The observed H_2 dependency of methane production was 1.01 and decreased with increasing carbon number to 0.84 for C_7 hydrocarbon. The observed CO dependency was -0.4 for methane and increased slightly with increasing carbon number. Assuming ASF of the distribution of the small-chain hydrocarbons, the chain growth probability α appeared to increase with increasing CO pressure and decreasing H_2 pressure. The reaction rates for n= 2-7 could be calculated with:

$$R_{C_n} = R_{CH_4} \alpha^{n-1} \tag{2.43}$$

The dependence of the chain growth probability factor α on CO and H_2 pressures has been correlated empirically [51, 143, 147, 172]. α increases with CO pressure, whereas an increase in H_2 pressure results in a minor or slight decrease of α. Empirical power law kinetics for paraffins as well as olefins have been proposed by Kellner and Bell [147], Bub and Baerns [143], and Anikeev et al. [172].

Several attempts to model these production rates more fundamentally have been reported [22, 73, 75, 101, 115, 118, 147, 148, 173]. Non-steady state kinetics obtained from step-concentration transients of (isotopic) feed components were used to measure absolute values of surface intermediates and intrinsic rate parameters [101, 173, 174]. Also steady state kinetic rates can be used to measure kinetic rate constants [18, 22, 75,

147]. Both approaches require a well-defined mechanistic scheme for the elementary reactions in the Fischer-Tropsch synthesis.

Bell [18] and Kellner and Bell [147] proposed a mechanism shown in Table 2.2. The kinetics were studied over an alumina-supported Ru catalyst. They assumed that CO is first adsorbed molecularly and subsequently gets dissociated. The Ru catalyst surface is assumed to be saturated with CO. It was assumed that the rate of methane formation is controlled by the hydrogenation of methyl, whereas chain growth and termination to higher paraffins and olefins are irreversible, and independent of the carbon number. The other reaction steps are at equilibrium. The probability of chain growth was given as

$$\alpha = \frac{k_p \theta_{CH_2}}{k_p \theta_{CH_2} + k_{t,O} \theta_v + k_{t,P} \theta_H} \tag{2.44}$$

Several simplifying assumptions were proposed in order to solve the kinetic equations and surface fraction of oxygen (θ_O) analytically. The olefin to paraffin ratio equaled $O/P \propto P_{H_2}^{-0.5}$. The authors observed a dependence of the O/P ratio with carbon number which they could not describe with their model. According to our opinion these discrepancies are due to readsorption or secondary reactions which were not taken into account. However, their kinetic expression for methane formation was approximately equal to the empirical dependency: $R_{CH_4} \propto P_{H_2}^{3/2} P_{CO}^{-1}$.

By assuming polymerization kinetics, Sarup and Wojciechowski [73] were able to derive kinetic rate expressions for the methanation and a mechanistic formulation for the paraffin formation based on the optimized model for the rate of CO consumption [168]. They made use of the polymerization kinetics where the rate of initiation must be equal to the rate of termination at steady state. The rate of initiation was equal to the hydrogenation of methylene to chain initiator methyl:

$$R_i = k_i \theta_H \theta_{CH_2} \tag{2.45}$$

and the rate of termination in their model was equal to the termination to paraffins due to hydrogenation (k_3) and reaction with a methyl species (k_4):

$$R_t = k_3 \theta_H \sum_1^\infty \theta_i + k_4 \theta_{CH_3} \sum_1^\infty \theta_i \tag{2.46}$$

Surface coverages of dissociated hydrogen (θ_H), methyl (θ_{CH_3}), alkyl chains (θ_i), and methylene (θ_{CH_2}) species were obtained using the assumption that the rate constant

for propagation as well as the rate constant for termination to paraffins is independent of chain length. Several other assumptions were introduced in order to derive dependencies of ratios of specific rates on P_{H_2} and P_{CO}. The approach of Sarup and Wojciechowski [73] is a good example how to combine the overall consumption rate of CO and a product distribution model. However, they use the concept of growth "locations" which is a number of sites in close proximity. E.g. formation of paraffins proceeds on three sites, the first site contains the growing alkyl chains, another the monomer and a final site contains a hydrogen atom that will result in termination and desorption of a paraffin. These locations are invariant with time and only small species can migrate towards the specific sites. Their approach involves a situation where a site can only contain one type of intermediate. In general, competitive adsorption of components on sites and surface diffusion of intermediates to sites will result in indistinguishable sites, without preference for certain types of intermediates. They also assumed two termination possibilities for paraffins to predict the "break" in the ASF distribution of paraffins. Rice and Wojciechowski [175] rejected the possibility of readsorption of olefins. However, several authors proved that olefins show a high tendency for secondary reactions and readsorption (see Chapter 2.7.2.2).

Zimmerman et al. [115] and Zimmerman [176] proposed a kinetic model for both the formation of linear olefins and paraffins and the water gas shift reaction. The model accounts for secondary readsorption of olefins on FT sites and the possibility of secondary hydrogenation of olefins on separate hydrogenation sites. The model was tested for a single experiment obtained with a commercial iron-based catalyst in a laboratory slurry reactor but showed significant deviations between model and experiments, specially for the methane and ethene content [115]. Their model predicts a decrease of the olefin to paraffin ratio and an increase of the chain growth factor with increasing chain length. The decrease is caused by the higher olefin concentration in the liquid. Zimmerman et al. [115] reported the following kinetic equations:

$$\text{Initiation: } R_i = k_p \theta_{CO} \theta_H^2 \tag{2.47}$$

$$\text{Propagation: } R_{p,i} = k_p \theta_i \theta_{CO} \theta_H \quad (i = 1 \rightarrow N) \tag{2.48}$$

Termination:

$$\text{methane } R_{t,P,1} = (k_{t,P} \theta_H + k_{t,O}) \theta_1 \tag{2.49}$$

$$\text{paraffins } R_{t,P,i} = k_{t,P} \theta_i \theta_H \quad (i = 2 \rightarrow N) \tag{2.50}$$

$$\text{olefins } R_{t,O,i} = k_{t,O} (\theta_i - P_{C_i H_{2i}} \theta_H / K_e) \quad (i = 2 \rightarrow N) \tag{2.51}$$

$$\text{Water gas shift: } R_{WGS} = k_w(P_{CO}P_{H_2O} - P_{CO_2}P_{H_2}/K_p) \tag{2.52}$$

$$\text{Olefin hydrogenation: } R_{s,i} = \frac{k_s P_{H_2} P_{C_i H_{2i}}}{1 + \left(K_{H_2} P_{H_2}\right)^{1/2} \left(1 + \sum_{i=1}^{N} K_e P_{C_i H_{2i}}\right)^2} \tag{2.53}$$

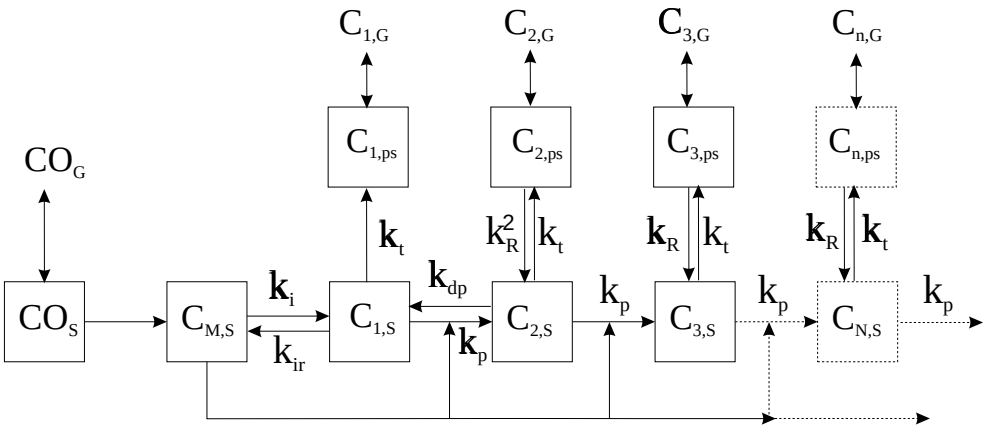

Figure 2.23 Chain growth model on Co catalyst (adapted from Komaya and Bell [101]).

Komaya and Bell [101] and Krishna and Bell [173] determined the pseudo reaction rate constants of the elementary FTS reactions over Ru/TiO_2 (T= 523 K) using both steady-state and transient-response kinetic experiments. Their pseudo rate constants contain surface concentrations of surface species and *real* kinetic rate constants. These pseudo kinetic rate constants will not only depend on temperature but also on pressure and composition. The chain growth model in Figure 2.23 was used as a basis for their kinetic models. In contrast to Krishna and Bell [173], Komaya and Bell [101] accounted for the effect of chain length dependent readsorption of olefins (k_R), as well as depolymerization of adsorbed ethylene (k_{dp}) and dehydrogenation of methyl to form a methylene monomer species (k_{ir}). Their explanation for increasing readsorption rates with carbon number is an increase of the physisorption strength with increasing carbon number. The observed rate coefficient of readsorption of ethene (k_R^2) is four orders of magnitude larger than for higher olefins. The authors did not specify separate termination reactions for the formation of paraffins and olefins from adsorbed alkyl species, but lumped the termination reactions in a single termination rate constant. Therefore, no influence of the partial pressures of CO and H_2 on the olefin to paraffin ratio was predicted.

Lox and Froment [75] developed a reaction network for the formation of linear hydrocarbons on a commercial precipitated iron catalyst. For each reaction path one or more elementary reaction steps were assumed to be slower than the other steps. On basis of the carbide mechanism they developed several kinetic models. Their experimental product distributions obtained at T= 523-623 K and H_2/CO= 3-6 in a fixed bed reactor at a high level of conversion fitted well with the Anderson-Schulz-Flory distribution. Their model predicts the desorption of products and adsorption of CO to be rate determining. The rate of formation for the paraffins is given by:

$$R_{C_nH_{2n+2}} = \frac{k_5 P_{H_2} \left(\frac{k_1 P_{CO}}{k_1 P_{CO} + k_5 P_{H_2}} \right) \alpha^{n-1}}{1 + \frac{1}{1-\alpha} \left(\frac{k_{HC1} P_{CO}}{k_1 P_{CO} + k_{HC5} P_{H_2}} \right)} \tag{2.54}$$

and for olefins:

$$R_{C_nH_{2n}} = \frac{k_6 \left(\frac{k_1 P_{CO}}{k_1 P_{CO} + k_5 P_{H_2}} \right) \alpha^{n-1}}{1 + \frac{1}{1-\alpha} \left(\frac{k_{HC1} P_{CO}}{k_1 P_{CO} + k_5 P_{H_2}} \right)} \tag{2.55}$$

with α given by:

$$\alpha = \frac{k_1 P_{CO}}{k_1 P_{CO} + k_5 P_{H_2} + k_6} \tag{2.56}$$

The growth probability factor α and the formation rates of the products depend on the partial pressure of CO and H_2 but are independent of the carbon number n. Their kinetic model predicts a constant ratio of the production rate of olefins to paraffins independent of the carbon number equal to:

$$\frac{R_{C_nH_{2n}}}{R_{C_nH_{2n+2}}} = \frac{m_{O_n}}{m_{P_n}} = \frac{k_6}{k_5 P_{H_2}} \tag{2.57}$$

Unfortunately, their experiments were performed in an integral packed bed reactor at high synthesis gas conversions, which is unsuitable for fundamental kinetic studies. Their product formation rates and models do not predict the well-known deviations observed in the nearly all FT product distributions.

Neither of the above-mentioned overall models is able to describe a detailed product distribution as a function of reactant pressures and operating conditions.

2.9 Conclusions

From the above we conclude that further research should concentrate on development of mechanistic rate expressions based on reliable mechanistic proposals. Coupling of the CO consumption and product distribution is an important feature of this new development. Until now, none of the available literature models obtains enough details to describe the complete product distribution of the Fischer-Tropsch synthesis at industrial conditions (high temperature and pressure) as a function of overall consumption of synthesis gas components and operating conditions. Either the product distribution model is oversimplified (Anderson-Schulz-Flory behavior), or the mechanistic proposals for the elementary reactions are unrealistic.

Rate equations for CO consumption to FT products show a great variety of inhibitor terms and are based on different mechanistic proposals. Also, many rate equations were proposed which are strongly influenced by the catalyst type and reaction conditions. The proposed FT kinetic equations on iron catalysts show inhibiting effects of CO_2 and H_2O, dependent on the WGS activity. However, close to equilibrium, a strong correlation between the inhibiting terms of CO_2 and H_2O occur. Rate equations based on a single-site rate determining reaction step between undissociated hydrogen and a carbon intermediate are presented for iron catalysts. On cobalt catalysts, dual-site elementary reactions between dissociated hydrogen and a carbon intermediate are considered to be the rate determining step. The majority of the kinetic rates under industrial conditions are reported per mass unit of catalyst. However, the preferred way to present rate data is in the form of specific activity, such as turnover rates (TOR) or frequencies (TOF). This way, different catalysts can be compared appropriately. Therefore, preparation and characterization procedures and calculations of surface area and metal dispersion should be reported in detail.

The WGS reaction is important for potassium-promoted iron catalysts at low H_2/CO ratios. Only a few authors reported on the WGS kinetics on iron catalysts under FT conditions. Therefore, development of WGS kinetic expressions from intrinsic kinetic experiments requires additional research.

The product distribution of the FTS shows significant deviations from the Anderson-Schulz-Flory distribution on iron, cobalt, and ruthenium catalysts. The ASF product distribution is changed by the occurrence of secondary reactions (hydrogenation, isomerization, reinsertion, and hydrogenolysis). Due to high CO and H_2O pressures present at FTS conditions, reinsertion of olefins appears to be the most important secondary reaction. The rates of these secondary reactions increase exponentially with

chain length. There is controversy in the literature about the fundamentals of these chain length dependency. Several possibilities for a chain length dependent contact time are physisorption, solubility and diffusivity. The chain length dependency of the olefin to paraffin ratio can hardly be due to diffusion effects only. Changes in the solubility and physisorption strength must be included in a proper model description. Reliable and independent measurements of these quantities on FT catalysts are necessary for the development of more accurate product distribution models.

Measured kinetic rates should not be influenced by deactivation of the catalyst. Experiments should be carried out in continuous perfectly mixed reactors (slurry or gas-solid) or differential fixed bed reactors over a wide range of independently varied experimental conditions. Kinetic experiments should preferably be accompanied by characterization measurements of the catalyst (for example different phases and texture). Process optimization and improvement of the FTS should result from kinetic equations for all products and reactants based on realistic mechanistic schemes. The development of new catalysts with high stability, activity and selectivity to the desired products is important. A model for a commercial reactor, which combines reliable kinetic expressions with hydrodynamics and mass transfer in a slurry bubble column should lead to improved scale up and development for industrial processes.

References

[1] Zimmerman, W.H.; Bukur, D.B., Effect of particle size on the activity of a fused iron Fischer-Tropsch catalyst, *Ind. Eng. Chem. Res.* **1989**, *28*, 406–413.

[2] Post, M.F.M.; van't Hoog, A.C.; Minderhoud, J.K.; Sie, S.T., Diffusion limitations in Fischer-Tropsch catalysts, *AIChE J.* **1989**, *35*, 1107–1114.

[3] Iglesia, E.; Reyes, S.C.; Soled, S.L., Reaction-transport selectivity models and the design of Fischer-Tropsch catalysts, in E.R. Becker; C.J. Pereira, eds., *Computer-aided design of catalysts*, Marcel Dekker, New York, 1993 pp. 199–257.

[4] Matthews, M.A.; Rodden, J.B.; Akgerman, A., High-temperature diffusion of hydrogen, carbon monoxide and carbon dioxide in liquid n-heptane, n-dodecane, and n-hexadecane, *J. Chem. Eng. Data* **1987**, *32*, 319–322.

[5] Albal, R.S.; Shah, Y.T.; Carr, N.L.; Bell, A.T., Mass transfer coefficients and solubilities for hydrogen and carbon monoxide under Fischer-Tropsch conditions, *Chem. Eng. Sci.* **1984**, *39*, 905.

[6] Ponec, V.; Van Barneveld, W.A., The role of chemisorption in Fischer-Tropsch synthesis, *Ind. Eng. Chem. Prod. Res. Des.* **1979**, *4*, 268–271.
[7] Rofer-De Poorter, C.K., A comprehensive mechanism for the Fischer-Tropsch synthesis, *Chem. Rev.* **1981**, *81*, 447–474.
[8] Vannice, M.A., The catalytic synthesis of hydrocarbons from H_2/CO mixtures over the group VIII metals. II. The kinetics of the methanation reaction over supported metals, *J. Catal.* **1975**, *37*, 462–473.
[9] Bond, G.C., *Catalysis by metals*, Academic Press, New York **1962**.
[10] Dry, M.E.; Shingles, T.; Boshoff, L.J.; Oosthuizen, G.J., Heats of adsorption on promoted iron surfaces and the role of alkali in Fischer-Tropsch synthesis, *J. Catal.* **1969**, *15*, 190–199.
[11] Vannice, M.A., The catalytic synthesis of hydrocarbons from carbon monoxide and hydrogen, *Catal. Rev.-Sci. Eng.* **1976**, *14*, 153–191.
[12] Röper, M., Fischer-Tropsch synthesis, in W. Keim, ed., *Catalysis in C_1 chemistry*, D. Reidel, Dordrecht, The Netherlands, 1983 pp. 41–88.
[13] Dry, M.E., The Fischer-Tropsch synthesis, in J.R. Anderson; M. Boudart, eds., *Catalysis-Science and technology*, vol. 1, Springer-Verlag, New York, 1981 pp. 160–255.
[14] Curtis Conner, Jr., W.; Falconer, J.L., Spillover in heterogeneous catalysts, *Chem. Rev.* **1995**, *95*, 759–788.
[15] Masel, R.I., *Principles of adsorption and reaction on solid surfaces*, Wiley & Sons, New York **1996**.
[16] Ponec, V., Some aspects of the methanation and Fischer-Tropsch synthesis, *Catal. Rev.-Sci. Eng.* **1978**, *18*, 151–171.
[17] Muetterties, E.L.; Stein, J., Mechanistic features of catalytic carbon monoxide hydrogenation reactions, *Chem. Rev.* **1979**, *79*, 479–490.
[18] Bell, A.T., Catalytic synthesis of hydrocarbons over group VIII metals. A discussion on the reaction mechanism, *Catal. Rev.-Sci. Eng.* **1981**, *23*, 203–232.
[19] Shustorovich, E., Metal effects in the Fischer-Tropsch synthesis: bond-order-conservation-morse-potential approach, *Catal. Lett.* **1990**, *7*, 107–118.
[20] Vannice, M.A., Catalytic activation of CO on metal surfaces, in J.R. Anderson; M. Boudart, eds., *Catalysis-Science and technology*, vol. 3, Springer-Verlag, New York, 1982 pp. 139–198.
[21] Van Santen, R.A.; Neurock, M., Concepts in theoretical heterogeneous catalytic reactivity, *Catal. Rev.-Sci. Eng.* **1995**, *37*, 557–698.
[22] Wojciechowski, B.W., The kinetics of the Fischer Tropsch synthesis, *Catal.*

Rev.-Sci. Eng. **1988**, *30*, 629–702.

[23] Biloen, P.; Sachtler, W.M.H., Mechanism of hydrocarbon synthesis over Fischer-Tropsch catalysts, *Adv. Catal.* **1981**, *30*, 165–216.

[24] Anderson, R.B., *Catalysts for the Fischer-Tropsch synthesis*, vol. 4, Van Nostrand Reinhold, New York **1956**.

[25] Rao, V.U.S.; Stiegel, G.J.; Cinquegrane, G.J.; Srivastave, R.D., Iron-based catalysts for slurry-phase Fischer-Tropsch process: Technology review, *Fuel Process. Technol.* **1992**, *30*, 83–107.

[26] Jager, B.; Espinoza, R., Advances in low-temperature Fischer-Tropsch synthesis, *Catal. Today* **1995**, *23*, 17–28.

[27] Kölbel, H; Ralek, M., The Fischer-Tropsch synthesis in the liquid phase, *Catal. Rev.-Sci. Eng.* **1980**, *21*, 225–274.

[28] Chaumette, P.; Courty, Ph.; Kiennemann, A.; Ernst, B., Higher alcohol and paraffin synthesis on cobalt based catalysts: comparison of mechanistic aspects, *Top. in Catal.* **1995**, *2*, 117–126.

[29] Frohning, C.D.; Kölbel, H. Ralek, M.; Rottig, W.; Schuur, F.; Schulz, H., Fischer-Tropsch-Synthese, in J. Falbe, ed., *Chemierohstoffe aus Kohle*, Georg Thieme Verlag, Stuttgart, 1977 pp. 219–299.

[30] Van der Burgt, M.J.; Van Leeuwen, C.J.; delÁmico, J.J.; Sie, S.T., The Shell Middle Distillate Synthesis process, in D.M. Bibby; C.D. Chang; R.F. Howe; S. Yurchak, eds., *Methane Conversion*, Elsevier Science, New York, 1988 pp. 473–482.

[31] Sie, S.T.; Senden, M.M.G.; Van Wechum, H.M.H., Conversion of natural gas to transportation fuels via the Shell Middle Destillate Synthesis process (SMDS), *Catal. Today* **1991**, *8*, 371–394.

[32] Madon, R.J.; Iglesia, E.; Reyes, S.C., Non-Flory product distributions in Fischer-Tropsch synthesis catalyzed by Ruthenium, Cobalt, and Iron, in S.L. Suib; M.E. Davis, eds., *Selectivity in Catalysis*, ACS Symposium Series, American Chemical Society, 1993 pp. 382–396.

[33] Berge van, P.J.; Everson, R.C., Cobalt as an alternative Fischer-Tropsch catalyst to iron for the production of middle distillates, *Stud. Surf. Sci. Catal.* **1997**, *107*, 207–212.

[34] Schulz, H., Polymethylen aus Synthesegas, in J. Falbe, ed., *Chemierohstoffe aus Kohle*, Georg Thieme Verlag, Stuttgart, 1977 pp. 335–355.

[35] Vannice, M.A., The catalytic synthesis of hydrocarbons from CO and H_2 over group VIII metals. V. The catalytic behavior of silica-supported metals, *J. Catal.*

1977, *50*, 228.

[36] Ernst, B.; Bensaddik, A.; Jilaire, L.; Chaumette, P.; Kienemann, A., Study on cobalt silica catalyst during reduction and Fischer- Tropsch reaction: In situ EXAFS compared to XPS and XRD, *Catal. Today* **1998**, *39*, 329–341.

[37] Rao, K.R.P.M.; Huggins, F.E.; Mahajan, V.; Huffman, G.P.; Rao, V.U.S.; Bhatt, B.L.; Bukur, D.B.; Davis, B.H.; O'Brien, R.J., Mössbauer spectroscopy study of iron-based catalysts used in Fischer-Tropsch synthesis, *Top. Catal.* **1995**, *2*, 71–78.

[38] Bukur, D.B.; Koranne, M.; Lang, X.; Rao, K.R.P.M.; Huffman, G.P., Pretreatment effect studies with a precipitated iron Fischer-Tropsch catalyst, *Appl. Catal. A* **1995**, *126*, 85–113.

[39] Lox, E.S.; Marin, G.B.; de Graeve, E.; Bussiere, P., Characterization of a promoted precipitated iron catalyst for Fischer-Tropsch synthesis, *Appl. Catal. A* **1988**, *40*, 197–218.

[40] Rao, K.R.P.M.; Huggins, F.E.; Huffman, G.P.; Gormley, R.J.; O'Brien, R.J.; Davis, B.H., Mössbauer spectroscopy study of iron Fischer-Tropsch catalysts during activation and synthesis, *Energy Fuels* **1996**, *10*, 546–551.

[41] Rao, K.R.P.M.; Huggins, F.E.; Mahajan, V.; Huffman, G.P.; Davis, B.; O'Brien, R.J.; Xu, L.; Rao, V.U.S., Effect of pre-heat treatment on a Fischer-Tropsch iron catalyst, *Hyperfine Interact.* **1994**, *93*, 1755–1758.

[42] Bukur, D.B.; Lang, X.; Rossin, J.A.; Zimmerman, W.H.; Rosynek, M.P.; Yeh, E.B.; Li, C., Activation studies with a promoted precipitated iron Fischer-Tropsch catalyst, *Ind. Eng. Chem. Res.* **1989**, *28*, 1130–1140.

[43] Bukur, D.B.; Okabe, K.; Rosynek, M.P.; Li, C.; Wang, D.; Rao, K.R.P.M.; Huffman, G.P., Activation studies with a precipitated iron catalyst for Fischer-Tropsch synthesis. 1. Characterization studies, *J. Catal.* **1995**, *155*, 353–365.

[44] Bukur, D.B.; Nowicki, L.; Manne, R.K.; Lang, X., Activation studies with a precipitated iron catalyst for Fischer-Tropsch synthesis 2. Reaction studies, *J. Catal.* **1995**, *155*, 366–375.

[45] Bukur, D.B.; Nowicki, L.; Patel, S.A., Activation studies with an iron Fischer-Tropsch catalyst in fixed bed stirred tank reactors, *Can. J. Chem. Eng.* **1996**, *74*, 399–404.

[46] Shroff, M.D.; Kalakkad, D.S.; Coulter, K.E.; Kòhler, S.D; Harrington, M.S.; Jackson, N.B.; Sault, A.G.; Datye, A.K., Activation of iron precipitated Fischer-Tropsch catalysts, *J. Catal.* **1995**, *156*, 185–207.

[47] Zhang, H.-B.; Schrader, G.L., Characterisation of a fused iron catalyst for

Fischer-Tropsch synthesis by in situ laser Raman spectroscopy, *J. Catal.* **1985**, *95*, 325–332.

[48] Van de Loosdrecht, J., *Preparation and properties of supported Fischer-Tropsch catalysts*, Ph.D. thesis, University of Utrecht, Utrecht, The Netherlands **1995**.

[49] Raupp, G.B.; Delgass, W.N., Mössbauer investigation of supported Fe catalysts. III In situ kinetics and spectroscopy during Fischer-Tropsch synthesis, *J. Catal.* **1979**, *58*, 361–369.

[50] Niemantsverdriet, J.W.; Van der Kraan, A.M.; Van Dijk, W.L.; Van der Baan, H.S., Behavior of metallic iron catalysts during Fischer-Tropsch synthesis studied with Mössbauer spectroscopy, X-ray diffraction, carbon content determination, and reaction kinetic measurements, *J. Phys. Chem.* **1980**, *84*, 3363–3370.

[51] Dictor, R.A.; Bell, A.T., Fischer-Tropsch synthesis over reduced and unreduced iron oxide catalysts, *J. Catal.* **1986**, *97*, 121–136.

[52] Amelse, J.A.; Butt, J.B.; Schwartz, L.H., Carburization of supported iron synthesis catalysts, *J. Phys. Chem.* **1978**, *82*, 558–563.

[53] Rao, K.R.P.M.; Huggins, F.E.; Mahajan, V.; Huffman, G.P.; Rao, V.U.S., Mössbauer spectroscopy study of CO-precipitated Fischer-Tropsch iron catalysts, *Hyperfine Interact.* **1994**, *93*, 1751–1754.

[54] Newsome, D.S., The water-gas shift reaction, *Catal. Rev.-Sci. Eng.* **1980**, *21*, 275–318.

[55] Satterfield, C.N.; Huff, Jr., G.A., Usefulness of a slurry-type Fischer-Tropsch reactor for processing synthesis gas of low hydrogen-carbon monoxide ratios, *Can. J. Chem. Eng.* **1982**, *60*, 159–162.

[56] Zimmerman, W.H.; Bukur, D.B., Reaction kinetics over iron catalysts used for the Fischer-Tropsch synthesis, *Can. J. Chem. Eng.* **1990**, *68*, 292–301.

[57] Lox, E.S.; Froment, G.F., Kinetics of the Fischer-Tropsch reaction on a precipitated promoted iron catalyst. 1. Experimental procedure and results, *Ind. Eng. Chem. Res.* **1993**, *32*, 61–70.

[58] Rethwisch, D.G.; Dumesic, J.A., Adsorptive and catalytic properties of supported metal oxides. III. Water-gas shift over supported iron and zinc oxides, *J. Catal.* **1986**, *101*, 35–42.

[59] Anderson, R.B., *The Fischer-Tropsch synthesis*, Academic Press, New York **1984**.

[60] Hindermann, J.P.; Hutchings, G.J.; Kiennemann, A., Mechanistic aspects of the formation of hydrocarbons and alcohols from CO hydrogenation, *Catal. Rev.-Sci. Eng.* **1993**, *35*, 1–127.

[61] Dry, M.E., Conversion of syngas to fuels and chemicals, in *Int. Conf. on Catal. & Catal. Proc.*, Cape Town, South Africa, 1993 pp. 57–66.

[62] Dry, M.E., Practical and theoretical aspects of the catalytic Fischer-Tropsch process, *Appl. Catal. A* **1996**, *138*, 319–344.

[63] Adesina, A.A., Hydrocarbon synthesis via Fischer-Tropsch reaction: travails and triumphs, *Appl. Catal. A* **1996**, *138*, 345–367.

[64] Schulz, H.; Beck, K.; Erich, E., Mechanism of the Fischer-Tropsch process, in D.M. Bibby; C.D. Chang; R.F. Howe; S. Yurchak, eds., *Methane Conversion*, Elsevier Science, 1988 pp. 457–471.

[65] Biloen, P.; Helle, J.N.; Sachtler, W.M.H., Incorporation of surface carbon into hydrocarbons during Fischer-Tropsch synthesis: mechanistic implications, *J. Catal.* **1979**, *58*, 95–107.

[66] Chuang, S.C.; Thian, Y.H.; Goodwin, Jr., J.G.; Wender, I., The use of probe moelcules in the study of CO hydrogenation over SiO_2-supported Ni,Ru, Rh, and Pd, *J. Catal.* **1985**, *96*, 396–407.

[67] Fischer, F.; Tropsch, H., Uber die Herstellung synthetischer ölgemische (Synthol) durch Aufbau aus Kohlenoxyd und Wasserstoff, *Brennst. Chem.* **1923**, *4*, 276–285.

[68] Schulz, H.; Van Steen, E.; Claeys, M., Olefin formation, hydrogenation and isomerization in the kinetic regime of Fischer-Tropsch synthesis, in *Selective hydrogenation and dehydrogenation*, DGMK, Kassel, Germany, 1993 .

[69] Kobori, Y.; Yamasaki, H.; Naito, S.; Onishi, T.; Tamaru, K., *J. Chem. Soc., Faraday Trans. 1* **1982**, *78*, 473.

[70] Biloen, P.; Helle, J.N.; van den Berg, F.G.A.; Sachtler, W.M.H., Mechanism of hydrocarbon synthesis over Fischer-Tropsch catalysts, *J. Catal.* **1983**, *81*, 450.

[71] Bianchi, D.; Tau, L.M.; Borcar, S.; Bennett, C.O., Nature of the species on supported iron during CO/H_2 reaction, *J. Catal.* **1983**, *84*, 358–374.

[72] Huff, Jr., G.A.; Satterfield, C.N., Intrinsic kinetics of the Fischer-Tropsch synthesis on a reduced fused-magnetite catalyst, *Ind. Eng. Chem. Process Des. Dev.* **1984**, *23*, 696–705.

[73] Sarup, B.; Wojciechowski, B.W., Studies of the Fischer-Tropsch synthesis on a cobalt catalyst. II. Kinetics of carbon monoxide conversion to methane and to higher hydrocarbons, *Can. J. Chem. Eng.* **1989**, *67*, 62–74.

[74] Schulz, H.; Beck, K.; Erich, E., Kinetics of Fischer-Tropsch selectivity, *Fuel Process. Technol.* **1988**, *18*, 293–304.

[75] Lox, E.S.; Froment, G.F., Kinetics of the Fischer-Tropsch reaction on a precip-

itated promoted iron catalyst. 2. Kinetic modeling, *Ind. Eng. Chem. Res.* **1993**, *32*, 71–82.

[76] Hovi, J.-P.; Lahtinen, J.; Liu, Z.S.; Nieminen, R.M., Monte Carlo study of CO hydrogenation on cobalt model catalysts, *J. Chem. Phys.* **1995**, *102*, 7674–7682.

[77] Novak, S.; Madon, R.J.; Suhl, H., Models of hydrocarbon product distributions in Fischer-Tropsch synthesis, *J. Chem. Phys.* **1981**, *74*, 6083–6091.

[78] Novak, S.; Madon, R.J.; Suhl, H., Secondary effects in the Fischer-Tropsch synthesis, *J. Catal.* **1982**, *77*, 141–151.

[79] Oki, S.; Mezaki, R., Identification of rate controlling steps for the water gas shift reaction over an iron catalyst, *J. Phys. Chem.* **1973a**, *77*, 447.

[80] Oki, S.; Mezaki, R., Mechanistic structure of the water gas shift reaction in the vicinity of chemical equilibrium, *J. Phys. Chem.* **1973b**, *77*, 1601.

[81] Grenoble, D.C.; Edstadt, M.M.; Ollis, D.F., The chemistry and catalysis of the water gas shift reaction, *J. Catal.* **1981**, *67*, 90–102.

[82] Graaf, G.H.; Winkelman, J.G.M.; Stamhuis, E.J.; Beenackers, A.A.C.M., Kinetics of the three-phase methanol synthesis, *Chem. Eng. Sci.* **1988**, *43*, 2161–2168.

[83] Chinchen, G.C.; Mansfield, K.; Spencer, M.S., The methanol synthesis: How does it work?, *CHEMTECH* **1990**, 241.

[84] Sachtler, W.H.M., Mechanismus der katalysierten Synthese von Kohlenwasserstoffen, *Chem.-Ing.-Tech.* **1982**, *54*, 901–907.

[85] Xu, J.; Froment, G.F., Methane steam reforming, methanation and water-gas shift: I. Intrinsic kinetics, *AIChE J.* **1989**, *35*, 88–96.

[86] Ovesen, C.V.; Clausen, B.S.; Hammershøi, B.S.; Steffensen, G.; Askgaard, T.; Chorkendorff, I.; Norskøv, J.K.; Rasmussen, P.B.; Stoltze, P.; Taylor, P., A microkinetic analysis of the water-gas-shift reaction under industrial conditions, *J. Catal.* **1996**, *158*, 170–180.

[87] Vandenbussche, K.M.; Froment, G.F., A steady-state kinetic model for methanol synthesis and the water gas shift reaction on a commercial $Cu/ZnO/Al_2O_3$ catalyst, *J. Catal.* **1996**, *161*, 1–10.

[88] Donnelly, T.J.; Yates, I.C.; Satterfield, C.N., Analysis and prediction of product distributions of the Fischer-Tropsch synthesis, *Energy Fuels* **1988**, *2*, 734–739.

[89] Iglesia, E.; Reyes, S.C.; Madon, R.J.; Soled, S.L., Selectivity control and catalyst design in the Fischer-Tropsch synthesis: sites, pellets, and reactors, in E.E. Eley; H. Pines; P.B. Weisz, eds., *Advances in Catalysis*, vol. 39, Academic Press, New York, 1993 pp. 221–302.

[90] Donnelly, T.J.; Satterfield, C.N., Product distributions of the Fischer-Tropsch synthesis on precipitated iron catalysts, *Appl. Catal. A* **1989**, *52*, 93–114.

[91] Bukur, D.B.; Patel, S.A.; Lang, X., Fixed bed and slurry reactor studies of Fischer-Tropsch synthesis on precipitated iron catalyst, *Appl. Catal. A* **1990**, *61*, 329–349.

[92] Kuipers, E.W.; Scheper, C.; Wilson, J.H.; Oosterbeek, H., Non-ASF product distributions due to secondary reactions during Fischer-Tropsch synthesis, *J. Catal.* **1996**, *158*, 288–300.

[93] Iglesia, E.; Reyes, S.C.; Madon, R.J., Transport-enhanced α-olefin readsorption pathways Ru-catalyzed hydrocarbon synthesis, *J. Catal.* **1991**, *129*, 238–256.

[94] Pichler, H.; Schulz, H., Neuere Erkentnisse auf dem Gebiet der Synthese von Kohlenwasserstoffen aus CO uns H_2, *Chem.-Ing.-Tech.* **1970**, *32*, 1162–1174.

[95] Dry, M.E., Catalytic aspects of industrial Fischer-Tropsch synthesis, *J. Mol. Catal.* **1982**, *17*, 133–144.

[96] Everson, R.C.; Woodburn, E.T.; Kirk, A.R.M., Fischer-Tropsch reaction studies with supported ruthenium catalysts I. product distributions at moderate pressures and catalyst deactivation, *J. Catal.* **1978**, *53*, 186–197.

[97] Glebov, L.S.; Kliger, G.A., The molecular weight distribution of the products of the Fischer-Tropsch synthesis, *Russ. Chem. Rev.* **1994**, *63*, 185–194.

[98] Puskas, I.; Hurlbut, R.S.; Pauls, R.E., Telomerization model for cobalt-catalyzed Fischer-Tropsch products, *J. Catal.* **1993**, *139*, 591–601.

[99] Huff, Jr., G.A.; Satterfield, C.N., Liquid accumulation in a Fischer-Tropsch fixed-bed reactor, *Ind. Eng. Chem. Process Des. Dev.* **1985**, *24*, 986–995.

[100] Sarup, B.; Wojciechowski, B.W., Studies of the Fischer-Tropsch synthesis on a cobalt catalyst. I. Evaluation of product distribution parameters from experimental data, *Can. J. Chem. Eng.* **1988**, *66*, 831–842.

[101] Komaya, T.; Bell, A.T., Estimates of rate coefficients for elementary processes occurring during Fischer-Tropsch synthesis over Ru/TiO_2, *J. Catal.* **1994**, *146*, 237–248.

[102] Jordan, D.S.; Bell, A.T., Influence of ethene on the hydrogenation of CO over ruthenium, *J. Phys. Chem.* **1986**, *90*, 4797–4805.

[103] Kuipers, E.W.; Vinkenburg, I.H.; Oosterbeek, H., Chain length dependence of α-olefin readsorption in Fischer-Tropsch synthesis, *J. Catal.* **1995**, *152*, 137–146.

[104] König, L.; Gaube, J., Fischer-Tropsch-Synthese. Neuere Untersuchungen und Entwickelungen, *Chem.-Ing.-Tech.* **1983**, *55*, 14–22.

[105] Egiebor, N.O.; Cooper, W.C.; Wojciechowski, B.W., Carbon number distribution of Fischer-Tropsch CO-hydrogenation products from precipitated iron catalysts, *Can. J. Chem. Eng.* **1985**, *63*, 826–834.

[106] Yates, I.C.; Satterfield, C.N., Hydrocarbon selectivity from cobalt Fischer-Tropsch catalysts, *Energy Fuels* **1992**, *6*, 308–314.

[107] Inoue, M.; Miyake, T.; Inui, T., Alcohol synthesis from syngas on ruthenium-based composite catalysts, *J. Catal.* **1987**, *105*, 266.

[108] Iglesia, E.; Vroman, H.; Soled, S.L.; Baumgartner, J.E.; Fiato, R.A., Selective catalysts and their preparation for catalytic hydrocarbon synthesis, *US Patent 5,036,032* **1991**.

[109] Huff, Jr., G.A.; Satterfield, C.N., Some kinetic design considerations in the Fischer-Tropsch synthesis on a reduced fused-magnetite catalyst, *Ind. Eng. Chem. Process Des. Dev.* **1984**, *23*, 851–854.

[110] Stenger, H.G.; Satterfield, C.N., Effect of liquid composition on the slurry Fischer-Tropsch synthesis. 1. Rate of reaction, *Ind. Eng. Chem. Process Des. Dev.* **1985**, *24*, 407–411.

[111] Bianchi, C.L.; Ragaini, V., Experimental evidence of α-olefin readsorption in Fischer-Tropsch synthesis on ruthenium-supported ETS-10 titanium silicate catalysts, *J. Catal.* **1997**, *168*, 70–74.

[112] Madon, R.J.; Iglesia, E., The importance of olefin readsorption and H_2/CO reactant ratio for hydrocarbon chain growth on ruthenium catalysts, *J. Catal.* **1993**, *139*, 576–590.

[113] Madon, R.J.; Reyes, S.C.; Iglesia, E., Primary and secondary reaction pathways in ruthenium-catalyzed hydrocarbon synthesis, *J. Phys. Chem.* **1991**, *95*, 7795–7804.

[114] Tau, L.-M.; Dabbagh, A.; Davis, B.H., Fischer-Tropsch synthesis: ^{14}C tracer study of alkene incorporation, *Energy Fuels* **1990**, *4*, 94–99.

[115] Zimmerman, W.H.; Bukur, D.B.; Ledakowicz, S., Kinetic model of Fischer-Tropsch selectivity in the slurry phase, *Chem. Eng. Sci.* **1992**, *47*, 2707–2712.

[116] Schulz, H.; Rao, B.R.; Elstner, M., ^{14}C-Studien zum Reaktionsmechnanismus der Fischer-Tropsch-Synthese, *Erdöl Kohle* **1970**, *23*, 651–655.

[117] Schulz, H.; Gökcebay, H., Fischer-Tropsch CO-hydrogenation as a means for linear olefins production, in J.R. Kosak, ed., *Catalysis of organic reactions*, Marcel Dekker, 1984 pp. 153–169.

[118] Schulz, H.; Steen van, E.; Claeys, M., Specific inhibition as the kinetic principle of the Fischer-Tropsch synthesis, *Top. Catal.* **1995**, *2*, 223–234.

[119] Hanlon, R.T.; Satterfield, C.N., Reactions of selected 1-olefins and ethanol added during the Fischer-Tropsch synthesis, *Energy Fuels* **1988**, *2*, 196–204.

[120] Jordan, D.S.; Bell, A.T., The influence of butene on CO hydrogenation over ruthenium, *J. Catal.* **1987**, *108*, 63–76.

[121] Jordan, D.S.; Bell, A.T., The influence of propylene on CO hydrogenation over silica-supported ruthenium, *J. Catal.* **1987**, *107*, 338–350.

[122] Dwyer, D.J.; Somorjai, G.A., The role of readsorption in determining the product distribution during CO hydrogenation over Fe single crystals, *J. Catal.* **1979**, *56*, 249–257.

[123] Dalla Betta, R.A.; Piken, A.G.; Shelef, M., Heterogeneous methanation: initial rate of CO hydrogenation on supported ruthenium and nickel, *J. Catal.* **1974**, *35*, 54.

[124] Pichler, H.; Schulz, H. Elstner, M., Gesetzmassigheiten bei der Synthese von Kohlenwasserstoffen aus Kohlenoxide und Wasserstoff, *Brennst. Ch.* **1967**, *48*, 78–87.

[125] Hall, W.K.; Kokes, R.J.; Emmett, P.H., Mechanism studies of the Fischer-Tropsch synthesis: the incorporation of radioactive ethylene, propionaldehyde and propanol, *J. Am. Chem. Soc.* **1960**, *82*, 1027–1037.

[126] Erkey, C.; Rodden, J.B.; Akgerman, A., Diffusivities of synthesis gas and n-alkanes in Fischer-Tropsch wax, *Energy Fuels* **1990**, *4*, 275–276.

[127] Reid, R.C.; Prausnitz, J.M.; Poling, B.E., *The properties of gases and liquids*, McGraw-Hill, New York, fourth edn. **1987**.

[128] Madon, R.J.; Iglesia, E., Hydrogen and CO intrapellet diffusion effects in ruthenium-catalyzed hydrocarbon synthesis, *J. Catal.* **1994**, *149*, 428–437.

[129] Breman, B.B.; Beenackers, A.A.C.M.; Rietjens, E.W.J.; Stege, R.J.H., Gas-liquid solubilities of carbon monoxide, carbon dioxide, hydrogen, water, 1-alcohols ($1 \leq n \leq 6$), and n-paraffins ($1 \leq n \leq 6$) in hexadecane, octacosane, 1-hexadecanol, phenantrene, and tetraethylene glycol at pressures up to 5.5 MPa and temperatures from 293 to 552 K, *J. Chem. Eng. Data* **1994**, *39*, 647–666.

[130] Chappelow, C.C.; Prausnitz, J.M., Solubilities of gases in high-boiling hydrocarbon solvents, *AIChE J.* **1974**, *20*, 1097–1103.

[131] Donohue, M.C.; Shah, D.S.; Connally, K.G.; Venkatachalam, V.R., Henry's constants for C_5 to C_9 hydrocarbons in C_{10} and larger hydrocarbons, *Ind. Eng. Chem. Fundam.* **1985**, *24*, 241–246.

[132] Caldwell, L.; van Vuuren, D.S., On the formation and composition of the liquid phase in Fischer-Tropsch reactors, *Chem. Eng. Sci.* **1986**, *41*, 89–96.

[133] Iglesia, E., Fischer-Tropsch synthesis on cobalt catalysts: structural requirements and reaction pathways, *Stud. Surf. Sci. Catal.* **1997**, *107*, 153–162.

[134] Eckert, C.A., Molecular thermodynamics of chemical reactions, *Ind. Eng. Chem.* **1967**, *59*, 20–32.

[135] Rybolt, T.R.; Wall, M.D.; Thomas, H.E.; Bramblett, J.W.; Phillips, M., Gas-solid chromatography and virial analysis of hydrocarbon adsorption on 13X zeolite, *J. Colloid Interface Sci.* **1990**, *138*, 113–121.

[136] Miyabe, K.; Suzuki, M., Solvent effect on adsorption phenomena in reversed-phase liquid chromatography, *AIChE J.* **1995**, *41*, 536–547.

[137] Miyabe, K.; Suzuki, M., Chromatographic study on liquid-phase adsorption on octadecylsilyl-silica gel, *AIChE J.* **1995**, *41*, 548–558.

[138] Keldsen, G.L.; Nicholas, J.B.; Carrado, K.A.; Winans, R.E., Molecular modeling of the enthalpies of hydrocarbons on smectite clay, *J. Phys. Chem.* **1994**, *98*, 279–284.

[139] Ruthven, D.M., *Principles of adsorption and adsorption processes*, Wiley & Sons, New York **1984**.

[140] Kiselev, A.V.; Shcherbakova, K.D., in *Molecular Sieves*, Proceedings of the First International Conference on Zeolites, Soc. Chem. Ind., London, 1967 .

[141] Xia, T.K.; Landman, U., Molecular dynamics of adsorption and segregation from an alkane mixture, *Science* **1993**, *261*, 1310–1312.

[142] Herrington, E.F.G., The Fischer-Tropsch synthesis considered as a polymerization reaction, *Chem. Ind.* **1946**, *65*, 346.

[143] Bub, G.; Baerns, M., Prediction of the performance of catalytic fixed bed reactors for Fischer-Tropsch synthesis, *Chem. Eng. Sci.* **1980**, *35*, 348–355.

[144] Dixit, R.S.; Tavlarides, L.L., Kinetics of the Fischer-Tropsch synthesis, *Ind. Eng. Chem. Process Des. Dev.* **1983**, *22*, 1–9.

[145] Nettelhoff, H.; Kokuun, R.; Ledakowicz, S.; Deckwer, W.-D., Studies on the kinetics of Fischer-Tropsch synthesis in slurry phase, *Ger. Chem. Eng.* **1985**, *8*, 177–185.

[146] Huff, Jr., G.A.; Satterfield, C.N., Stirred autoclave apparatus for study of the Fischer-Tropsch synthesis in a slurry bed. 2. Analytical procedures, *Ind. Eng. Chem. Fundam.* **1983**, *22*, 258–263.

[147] Kellner, C.S.; Bell, A.T., The kinetics and mechanism of carbon monoxide hydrogenation over alumina-supported ruthenium, *J. Catal.* **1981**, *70*, 418–432.

[148] Takoudis, C.G., Power rate law studies in heterogeneously catalyzed reactions, *Ind. Eng. Chem. Prod. Res. Dev.* **1984**, *23*, 149–153.

[149] Falbe, J.; Frohning, C.D., The raw materials future: critical examination of the role played by catalysis, *J. Mol. Catal.* **1982**, *17*, 117–132.

[150] Ribeiro, F.H.; Schach von Wittenau, A.E.; Bartholemew, C.H.; Somorjai, G.A., Reproducibility of turnover rates in heterogeneous metal catalysis: compilation of data and guidelines for data analysis, *Catal. Rev.-Sci. Eng.* **1997**, *39*, 49–76.

[151] Martin-Martinez, J.M.; Vannice, M.A., Carbon-supported iron catalysts: Influence of support porosity and preparation techniques on crystallite size and catalytic behavior, *Ind. Eng. Chem. Res.* **1991**, *30*, 2263–2275.

[152] Snel, R., Supported iron catalysts in Fischer-Tropsch synthesis: Influence of the preparation method, *Ind. Eng. Chem. Res.* **1989**, *28*, 654–659.

[153] Roe, G.M.; Ridd, M.J.; Cavell, K.J.; Larkins, F.P., Role of supports for cobalt-based catalysts used in Fischer-Tropsch synthesis of hydrocarbons, in D.M. Bibby; C.D. Chang; R.F. Howe; S. Yurchak, eds., *Methane Conversion*, Elsevier Science, 1988 pp. 509–515.

[154] Iglesia, E.; Soled, S.L.; Fiato, R.A., Fischer-Tropsch synthesis on cobalt and ruthenium. Metal dispersion and support effects on reaction rate and selectivity, *J. Catal.* **1992**, *137*, 212–224.

[155] Dry, M.E.; Shingles, T.; Boshoff, L.J.; Oosthuizen, G.J., Rate of the Fischer-Tropsch reaction over iron catalysts, *J. Catal.* **1972**, *25*, 99–104.

[156] Dry, M.E., Advances in Fischer-Tropsch chemistry, *Ind. Eng. Chem. Prod. Res. Dev.* **1976**, *15*, 282–286.

[157] Atwood, H.E.; Bennett, C.O., Kinetics of the Fischer-Tropsch reaction over iron, *Ind. Eng. Chem. Process Des. Dev.* **1979**, *18*, 163–170.

[158] Shen, W.J.; Zhou, J.L.; Zhang, B.J., Kinetics of Fischer-Tropsch synthesis over precipitated iron catalyst, *J. Nat. Gas Chem.* **1994**, *4*, 385–400.

[159] Deckwer, W.-D.; Kokuun, R.; Sanders, E.; Ledakowicz, S., Kinetic studies of Fischer-Tropsch synthesis on suspended Fe/K catalyst. Rate inhibition by CO_2 and H_2O, *Ind. Eng. Chem. Process Des. Dev.* **1986**, *25*, 643–649.

[160] Whiters, Jr., H.P.; Eleizer, K.F.; Mitchell, J.W., Slurry-phase Fischer-Tropsch synthesis and kinetic studies over supported cobalt carbonyl derived catalysts, *Ind. Eng. Chem. Res.* **1990**, *29*, 1807–1814.

[161] Ledakowicz, S.; Nettelhoff, H.; Kokuun, R.; Deckwer, W.-D., Kinetics of the Fischer-Tropsch synthesis in the slurry phase on a potassium-promoted iron catalyst, *Top. Catal.* **1985**, *24*, 1043–1049.

[162] Chanenchuk, C.A.; Yates, I.C.; Satterfield, C.N., The Fischer-Tropsch synthesis with a mechanical mixture of a cobalt catalyst and a copper-based water gas

shift catalyst, *Energy Fuels* **1991**, *5*, 847–855.

[163] Yates, I.C.; Satterfield, C.N., Intrinsic kinetics of the Fischer-Tropsch synthesis on a cobalt catalyst, *Energy Fuels* **1991**, *5*, 168–173.

[164] Satterfield, C.N.; Hanlon, R.T.; Tung, S.E.; Zou, Z.; Papaefthymiou, G.C., Effect of water on the iron-catalyzed Fischer-Tropsch synthesis, *Ind. Eng. Chem. Prod. Res. Dev.* **1986**, *25*, 407–414.

[165] Boudart, M., Two-step catalytic reactions, *AIChE J.* **1972**, *18*, 465–478.

[166] Boelee, J.H., *The Fischer-Tropsch synthesis in slurry phase reactors. Kinetics and mass transfer*, Ph.D. thesis, University of Eindhoven, Eindhoven, The Netherlands **1988**.

[167] Yates, I.C.; Satterfield, C.N., Effect of carbon dioxide on the kinetics of the Fischer-Tropsch synthesis on iron catalysts, *Ind. Eng. Chem. Res.* **1989**, *28*, 9–12.

[168] Sarup, B.; Wojciechowski, B.W., Studies of the Fischer-Tropsch synthesis on a cobalt catalyst. III. Mechanistic formulation of the kinetics of selectivity for hydrocarbon formation, *Can. J. Chem. Eng.* **1989**, *67*, 620–627.

[169] Rofer-De Poorter, C.K., Untangling the water gas shift from Fischer-Tropsch: a gordian knot?, in R.G. Herman, ed., *Catalytic conversion of synthesis gas and alcohols to chemicals*, Plenum Press, New York, 1984 .

[170] Feimer, J.L.; Silveston, P.L.; Hudgins, R.R., Steady-state study of the Fischer-Tropsch reaction, *Ind. Eng. Chem. Prod. Res. Dev.* **1981**, *20*, 609–615.

[171] Graaf, G.H.; Sijtsema, P.J.J.M.; Stamhuis, E.J.; Joosten, G.E.H., Chemical equilibria in methanol synthesis, *Chem. Eng. Sci.* **1986**, *41*, 2883–2890.

[172] Anikeev, V.I.; Yermakova, A.; Gudkov, A.Y., Energy-chemical coal processing. 3. Fischer-Tropsch synthesis of light and heavy hydrocarbon fuels from coal gasification products, *Chem. Sust. Dev.* **1996**, *4*, 119–129.

[173] Krishna, K.R.; Bell, A.T., Estimates of the rate coefficients for chain initiation, propagation, and termination during Fischer-Tropsch synthesis over Ru/TiO_2, *J. Catal.* **1993**, *139*, 104–118.

[174] Zhang, X.; Biloen, P., A transient kinetic observation of chain growth in the Fischer-Tropsch synthesis, *J. Catal.* **1986**, *98*, 468–476.

[175] Rice, N.M.; Wojciechowski, B.W., On interpreting FT product distribution data, *Can. J. Chem. Eng.* **1987**, *65*, 102–112.

[176] Zimmerman, W.H., *Kinetic modeling of the Fischer-Tropsch synthesis*, Ph.D. thesis, Texas A&M University, College Station TX, USA **1990**.